L-750

NATIONAL ADVISORY COMMITTEE FOR AERONAUTICS

WARTIME REPORT

ORIGINALLY ISSUED
June 1944 as
Memorandum Report

STATIC-THRUST AND TORQUE CHARACTERISTICS OF SINGLE- AND DUAL-ROTATING TRACTOR PROPELLERS

By Jean Gilman, Jr.

Langley Memorial Aeronautical Laboratory
Langley Field, Va.

JPL LIBRARY
CALIFORNIA INSTITUTE OF TECHNOLOGY

NACA

WASHINGTON

NACA WARTIME REPORTS are reprints of papers originally issued to provide rapid distribution of advance research results to an authorized group requiring them for the war effort. They were previously held under a security status but are now unclassified. Some of these reports were not technically edited. All have been reproduced without change in order to expedite general distribution.

NATIONAL ADVISORY COMMITTEE FOR AERONAUTICS

MEMORANDUM REPORT

for the

Bureau of Aeronautics, Navy Department

STATIC-THRUST AND TORQUE CHARACTERISTICS OF SINGLE- AND DUAL-ROTATING TRACTOR PROPELLERS

By Jean Gilman, Jr.

SUMMARY

A program of outdoor tests was carried out to determine the static-thrust and torque characteristics of single- and dual-rotating propellers for use in aircraft propeller design and in take-off performance estimation. The propellers used for the tests were 10 feet in diameter and were made up of blades of Hamilton Standard design, drawing numbers 3155-6 and 3155-6-1.5. The characteristics were investigated over a considerable range of solidity for both single- and dual-rotating propellers. Blade-angle settings ranged from 10° to 40° in 5° increments.

The propeller characteristics are presented as functions of the blade-angle setting at the three-quarters radius and, for some comparisons, as a function of the power coefficient. Design charts showing the variation of thrust with total activity factor are included.

Dual-rotating propellers showed substantially higher static-thrust and power absorption than the corresponding single-rotating propellers. At equal power absorption the static thrust of the six-blade dual-rotating propeller was approximately equal to that of the eight-blade single-rotating propeller, both with standard-width blades. A wide-blade single-rotating propeller produced a slightly higher static thrust than did the propeller of equal solidity with standard-width blades. Faired data from the extrapolation of wind-tunnel test curves to zero V/nD were found to be generally consistent and of sufficient accuracy for use in most preliminary propeller calculations.

INTRODUCTION

The static-thrust and torque characteristics of aircraft propellers are often required in take-off calculations and propeller selection. Since only a limited amount of static-test data is available (reference 1), the data are usually obtained by the extrapolation of wind-tunnel test curves to zero advance-diameter ratio. Data obtained by this method, while generally satisfactory, have sometimes led to conflicting conclusions mainly because of the sparsity of data at low airspeeds.

In order to obtain true static condition and to avoid the undesirable features of indoor testing, a balance rig was constructed to permit outdoor testing. The identical propeller-nacelle combination used in references 2 and 3 was used in the outdoor tests at the NACA propeller-research tunnel to expand the scope of available information and to permit the direct comparison of the actual static-test results with those extrapolated from wind-tunnel tests.

The program covered tests of two-, three-, four-, six-, and eight-blade single-rotating and four-, six-, and eight-blade dual-rotating propellers of standard-blade width. In addition, three- and four-blade single-rotating and six- and eight-blade dual-rotating propellers of 50 percent increase in thickness and blade width were included. The blade-angle range was from 10° to 40°.

METHODS AND APPARATUS

A general idea of the test setup is given by figure 1. By following through the linkages indicated in figure 2, it may be seen that the balance reading difference was proportional to the thrust by a ratio of the moment arms ac/bd. The thrust measured in this way included a negative component due to the drag of the nacelle body and supports in the propeller slipstream. Calculations based on test data of reference 2 from wind-tunnel drag runs of the nacelle body alone indicated that this drag was 1.2 percent of the measured thrust.

The engine-nacelle body and propellers were those used in the previously mentioned wind-tunnel tests. (See references 2 and 3.) The motor arrangement and the spring-selsyn dynamometer used to measure the torque are described in reference 2. Dimensional details of the nacelle from reference 2 are reproduced in figure 3. The propellers were of 10-foot diameter, Hamilton Standard design with drawing numbers 3155-6 for the right hand and 3156-6 for the left-hand blades and with Clark Y sections throughout. Also included were propellers of the same diameter, blade sections, pitch distribution, and thickness ratio, but with blades 50 percent wider and thicker. These will hereafter be referred to as "wide blades," and the drawing numbers are modified to 3155-6-1.5 and 3156-6-1.5. Blade-form curves for both standard-width and wide blades are given in figure 4.

Check tests, with and without spinners, showed a negligible difference in the propeller characteristics for the static condition. A considerable saving of time in changing blade angles was effected in these tests by omitting the spinner surface.

Two-, three-, and four-blade single-rotating propellers were tested with the blades in the rear hub. The six- and eight-blade single- and dual-rotating propellers were made up on two hubs in tandem, each hub having an equal number of blades. The hub spacing was 10 inches for both single and dual rotation.

The position of the shaft splines prevented equiangular spacing of the blades for the six- and eight-blade single-rotating propellers. The front blades led the rear blades by 75° for the six-blade propeller and 52.5° for the eight-blade propeller. Results of reference 4 indicate that this unequal spacing would not affect the results.

The dual-rotating runs were made at equal front and rear propeller rotational speeds with the blades of the front component set in equal increments of 5° each but with the rear component adjusted to a slightly smaller angle. The differential settings, which are those giving approximately equal front and rear torque at peak efficiency, are given in figure 5. These settings were used because normally the flight efficiency of the propeller is of primary importance and also because the static tests are to supplement previously published wind-tunnel data. (See references 2 and 3.)

Blade angles were varied from 10° to 40° in 5° increments, with the exception that dual-rotating propellers with wide blades were not tested beyond 35° because the 10-inch hub spacing did not permit passage of the blades at higher settings.

At each blade-setting, several readings of thrust and torque were made over a small range of rpm. The test points thus obtained were plotted against rpm as shown in figure 6, faired, and the faired value was corrected for wind velocity.

The low power of the electric propeller-drive motors (two 25-horsepower induction motors) prevented any sensible occurrence of compressibility effects. The highest rotational speed (550 rpm at low blade angles only) resulted in a maximum attainable ratio of tip speed to the velocity of sound of 0.23.

The Reynolds number varied depending on the blade width and on the rotational speed obtainable. Based on the chord at 0.75 R, it was of the order of 900,000 for the standard-width blades.

Tests were made outdoors sufficiently far away from buildings or other obstructions that might have affected the flow. The limiting wind velocity beyond which testing was not done was taken as 5 miles per hour, plus or minus (plus or minus in the sense that a small positive or negative V/nD would result). Readings of wind velocity taken before and after each run on a vane-type anemometer were averaged in making the small corrections to the observed results. Testing in cross winds was avoided.

The accuracy of static-thrust tests conducted outdoors is lower than the wind-tunnel tests, partly because at the higher blade angles any wind velocity would have the effect of stalling or unstalling a portion of the blades, depending on its magnitude and direction relative to the normal induced inflow velocity. This fact would make any method of correction to actual static conditions less reliable, and is a source of possible error not present in wind-tunnel tests.

RESULTS AND DISCUSSION

The results are reduced to dimensionless coefficients as follows:

$$C_T = \frac{T_e}{\rho n^2 D^4}$$

$$C_P = \frac{2\pi n\, Q}{\rho n^3 D^5} = \frac{P}{\rho n^3 D^5}$$

$$C_{P_F} = \frac{2\pi n\, Q_F}{\rho n^3 D^5}$$

$$C_{P_R} = \frac{2\pi n\, Q_R}{\rho n^3 D^5}$$

C_{P_F}, C_{P_R} subscripts F and R refer to front and rear components of dual-rotating propellers

C_T/C_P static-thrust figure of merit

V/nD advance-diameter ratio

Standard NACA symbols are used:

T tension in propeller shaft, pounds

ΔD additional drag of nacelle and struts caused by propeller slipstream, pounds

$T_e = T - \Delta D$ effective thrust, pounds

P power absorbed by propeller, foot-pounds per second

Q propeller torque, pound-feet

n propeller rotational speed, revolutions per second

D propeller diameter, feet

ρ mass density of air, slugs per cubic foot

R propeller radius, feet

β blade angle at 0.75R, degrees

The results are presented in plots showing the propeller characteristics as a function of the blade-angle setting at the 0.75R. Comparisons are made on the basis of both blade-angle setting and power coefficient. Table I is a complete list of the figures giving these results.

The basic static characteristics are presented in figures 7 through 18, which are plots of C_T, C_P, and the ratio of C_T/C_P against blade angle. The scattering of the points, which are shown on the C_T and C_P curves, is usually less than 2 percent at blade angles less than 20°. Above 20° the dispersal is as much as 5 percent, which may be attributed to the previously cited wind effect.

The static-thrust figure of merit, C_T/C_P, is of practical utility in that it can be used to find the static thrust if the propeller diameter, engine power, and rpm are known because

$$C_T/C_P = T_e nD/P$$

This is a convenient form for dealing with controllable-pitch propellers where n is substantially constant. The effect of differences of propeller-body combination on ΔD, however, should be taken into account.

Figures 19 and 20 show the variation of power absorption with blade angle of the front and rear components of the six-blade dual-rotating propellers. Four- and eight-blade propeller results were similar. The coefficients for the front and rear components could have been made equal by setting the blades for equal power absorption at the static-thrust condition instead of at maximum efficiency. Reference 5 (fig. 36) indicates that negligible increase in static thrust would result. It should be remarked that the data from which figures 19 and 20 were prepared were not corrected for wind velocity

since this correction is very small. The sum of C_{P_F} and C_{P_R} therefore will not necessarily be equal to C_P.

Composites of the characteristic curves are presented in figures 21 and 22. It is to be expected that the thrust or power absorption of propellers would not vary directly with solidity or activity factor because of blade interference, and these curves are of particular interest in connection with this point because of the wide variation of solidity. The fact that the solidity was varied in two different ways is of further interest, as will be more fully illustrated.

Figure 21(a) presents curves of C_T as a function of blade angle for the standard-width propellers. These curves show the gain in static thrust resulting from increasing the number of blades. Increasing the number of blades also tends to delay the stall. Dual rotation increases the thrust and gives a less severe stall than the single-rotating propeller of corresponding solidity. The curves of C_T versus blade angle for the wide-blade propellers are shown in figure 21(b). No stalling was apparent for the six- and eight-blade dual-rotating propellers in the range of blade angles tested.

Figures 22(a) and (b) are composites of the power-coefficient curves, which show how the power absorption increases with increasing number of blades. The greater power absorption of the dual-rotating propellers, as compared to that of the corresponding single-rotating propellers, is evident. The four-blade single-rotating propellers, both with standard-width and wide blades, show a lessening of the rate of increase of power absorption starting between 25° and 30°, which may be the effect of blade interference. It would appear from this reasoning that the addition of more blades would accentuate this effect, but the power-coefficient curves of the six- and eight-blade singlerotating propellers do not show the effect to the same degree as the power-coefficient curve of the four-blade propeller. Both the six- and eight-blade propellers were tandem arrangements, however, which may have reduced the effect of blade interference at zero V/nD.

In figure 23 a comparison is made of two single-rotating propellers of equal solidity, but with one propeller having four wide and the other having six standard-width blades. Over the lower part of the blade-angle range, the power absorption of the wide-blade propeller is slightly less, but it becomes slightly greater at the higher blade angles. The static thrust of the four-blade propeller, however, is slightly higher throughout most of the blade-angle range. Some of the differences noted above could be ascribed to Reynolds number effect, since both propellers were run at approximately equal rotational speeds at equal blade angles. It is also possible that some of the differences were caused by the higher local inflow velocity of the wide-blade propeller which would reduce the blade element angles of attack and so delay the stall. A more practical comparison of these two propellers is given in figure 24 where C_T/C_P is plotted as a function of C_P. The higher static thrust of the wide-blade propeller over most of the range tested is thus shown.

A comparison of C_T/C_P of the eight-blade single-rotating with the six-blade dual-rotating propeller at equal power absorption, both propellers having standard-width blades, is given in figure 25. These curves indicate that the six-blade dual-rotating propeller produces more thrust at the higher power coefficients than does the eight-blade single-rotating propeller, in spite of the difference in solidity.

The variation of C_T with total activity factor at several values of C_P is given in figure 26. Figure 26(a) shows that the single-rotating wide-blade propellers produced a higher thrust for a given power than the corresponding propellers of standard-width blades. It appears from figure 26(b), however, that the difference between dual-rotating propellers of wide or standard-width blades is not so pronounced as in the single-rotating case. The curves of dual-rotating propellers having wide and standard-width blades are practically continuous up to a power coefficient of about 0.6. As a first approximation the thrust coefficient is the same for either propeller at a given total activity factor.

COMPARISON OF STATIC TEST AND EXTRAPOLATED WIND-TUNNEL RESULTS

Static-thrust and power characteristics have been useful chiefly for estimating the length of take-off run and for calculating nosing-over moments. Static-test data are usually unavailable for any particular propeller design and hence these data are usually obtained by the extrapolation of wind-tunnel test curves to zero V/nD. This method has been fairly satisfactory, but there may be some question as to the reliability of this method in the light of the recent development of aircraft engines of 2000 or more horsepower. Several factors such as dual rotation, propellers of high solidity, two-speed gearing, and combinations of these devices have come into prominence as means of efficiently absorbing this increased power at zero and low airspeeds. Reliable data are essential in properly evaluating the effect of variations in these schemes.

The fact that many combinations of single- and dual-rotating propellers had been previously tested in a wind-tunnel presented an opportunity to compare extrapolated results with test results. First, C_T and C_P points at zero V/nD were obtained by extrapolation, and inconsistencies were faired out after plotting these points against blade angle. Curves of C_T and C_P versus blade angle obtained in this manner were then superimposed on the test curves, as shown in figures 27 and 28. The agreement between results from static tests and those from the extrapolation of wind-tunnel test results is good in some cases and only fair in others. An important quantity in the application of these results is C_T/C_P. In figure 29 some of the results are compared on this basis as a function of blade angle. The largest variation appears in the curves of the four- and six-blade single-rotating propellers. In the case of the four-blade propeller, for example, the extrapolated value of C_T/C_P varies from 4 to 8 percent too high at the lower blade angles to as much as 19 percent too high at the higher blade angles.

Where possible, the wind-tunnel values without wing were used in order to correspond to the static-thrust results. In almost every case, however, the wind-tunnel

tests for the standard-width blades at 10° and 15° blade angle had been made only with the wing in place, but at these low blade angles the twist in the slipstream would be small so that the effect of a wing on a tractor propeller would be negligible. From 20° on, these blades had been tested both with and without wing, thus permitting comparison under the same condition as the static tests. Unfortunately, the wide blades had been tested only with wing through the entire blade-angle range. Nevertheless, it seemed that the wide-blade comparisons would still be of interest.

It was shown in reference 2 that the presence of a wing in the slipstream reduced the rotational losses of a single-rotating tractor propeller approximately 50 percent. From the above statement it would be expected that the values of C_T from the static tests of the wide-blade single-rotating propellers with no wing would be somewhat lower than the values from the wind-tunnel tests made with the wing, particularly at the higher blade angles where the twist of the slipstream is more pronounced. This result is definitely indicated in figure 27(c) by the C_T curves of the three- and four-blade single-rotating propellers with wide blades. A similar effect would not be anticipated for dual rotation, because the rear component of the propeller would tend to remove the twist of the slipstream. This is confirmed by the plots of the six- and eight-blade dual-rotating propellers with wide blades (fig. 27(d)).

The general uniformity of extrapolated wind-tunnel data as found in this investigation suggests that a more accurate picture of the effect of a wing on a tractor propeller might be obtained by comparisons based entirely on such data rather than basing the comparisons partly on static-test and partly on extrapolated wind-tunnel data. In figures 30 and 31, use is made of data from the extrapolation of wind-tunnel test results of the six-blade single- and dual-rotating propellers both with and without wing. (Data from reference 2.) At a value of C_P of 0.675, for example, C_T for the dual-rotating propeller is 0.427 either with or without wing, while, for the single-rotating propeller, C_T is 0.357 with wing and 0.309 without wing. At this value of C_P of 0.675, the wing increased the static-thrust coefficient of the single-rotating propeller by about 15 percent, but dual-rotation showed an increase over single rotation

(without wing) of about 38 percent. The effect of the wing on single-rotating propellers, however, is negligible at blade angles representative of the take-off condition, usually less than 30°.

CONCLUSIONS

The following conclusions are based on static-thrust comparisons free of compressibility effects. In the case of the dual-rotating propellers the pitch settings were adjusted to provide equal torque and power at peak efficiency.

1. Dual-rotating propellers exhibited a substantial gain in static thrust and power absorption over the corresponding single-rotating propellers.

2. On the basis of equal power absorption, the six-blade dual-rotating propeller was found to be capable of producing approximately the same static thrust as the eight-blade single-rotating propeller, both propellers having standard-width blades.

3. At equal solidity or total activity factor, wide-blade single-rotating propellers produced a higher static thrust for a given power coefficient than did the equivalent propellers with standard-width blades.

4. The agreement of C_T/C_P as obtained from static-test and extrapolated results of wind-tunnel tests, while generally fair, was found in one case to vary as much as 19 percent.

Langley Memorial Aeronautical Laboratory
National Advisory Committee for Aeronautics
Langley Field, Va., June 28, 1944

REFERENCES

1. Hartman, Edwin P., and Biermann, David: Static Thrust and Power Characteristics of Six Full-Scale Propellers. NACA Rep. No. 684, 1940.

2. Biermann, David, and Hartman, Edwin P.: Wind-Tunnel Tests of Four- and Six-Blade Single- and Dual-Rotating Tractor Propellers. NACA Rep. No. 747, 1942.

3. Gray, W. H., and Mastrocola, Nicholas: Representative Operating Charts of Propellers Tested in the NACA 20-Foot Propeller-Research Tunnel. NACA ARR No. 3I25, 1943.

4. Biermann, David, and Conway, Robert N.: Wind-Tunnel Tests of Propellers Having a Biplane Arrangement of the Blades. NACA ARR, March 1942.

5. Gray, W. H. Wind-Tunnel Tests of Dual-Rotating Propellers with Systematic Differences in Number of Blades, Blade Setting, and Rotational Speed of Front and Rear Propellers. NACA ARR No. L4E22, 1944.

TABLE I

LIST OF FIGURES

Figure	Description	Number of blades	Blade width	Rotation
7	Static characteristics	2	Standard	Single
8		3	Standard	Single
9		3	Wide	Single
10		4	Standard	Single
11		4	Standard	Dual
12		4	Wide	Single
13		6	Standard	Single
14		6	Standard	Dual
15		6	Wide	Dual
16		8	Standard	Single
17		8	Standard	Dual
18		8	Wide	Dual
19,20	Power absorption of front and rear components of six-blade dual-rotating propellers			
21,22	Composites of static characteristics			
23,24	Comparisons at equal solidity			
25	Comparison of single and dual rotation.			
26	Activity factor charts			
27-29	Comparison of extrapolated and test data			
30,31	Effect of wing in slip stream			

L-750

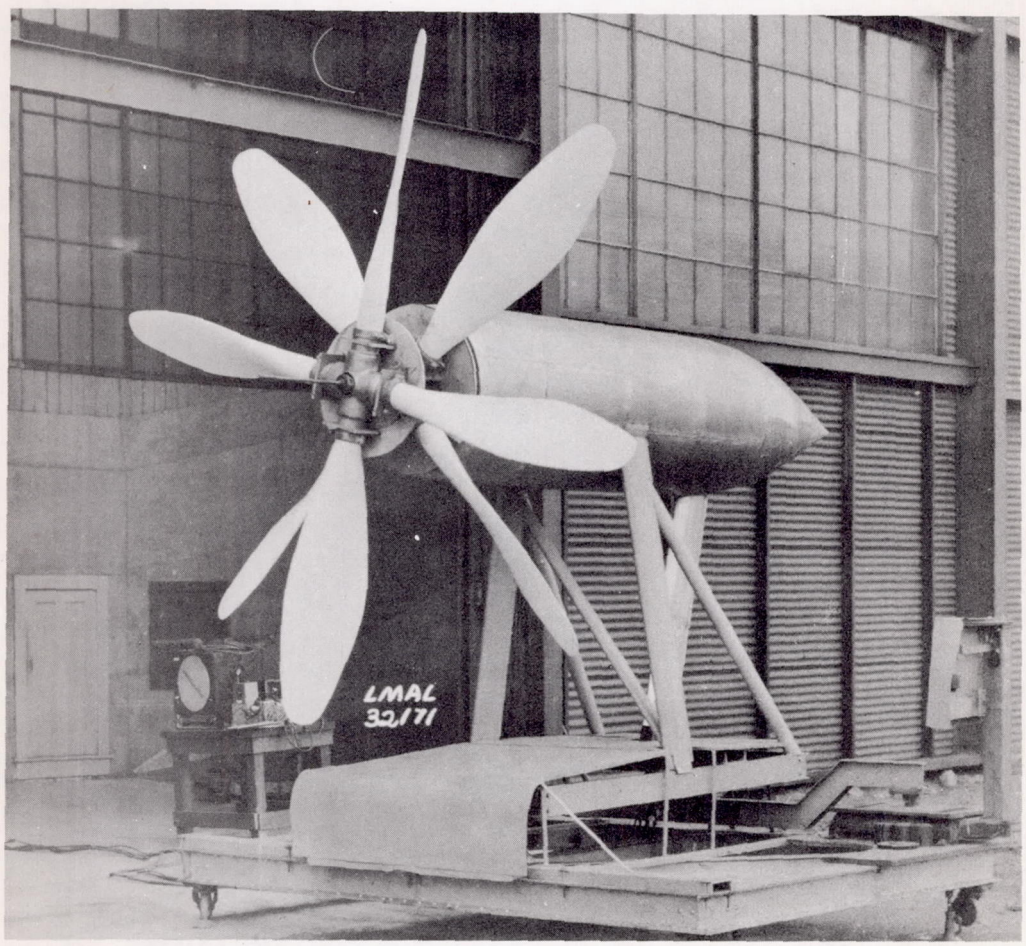


Figure 1.- Static-thrust test setup, with eight wide blades, arranged for dual rotation.

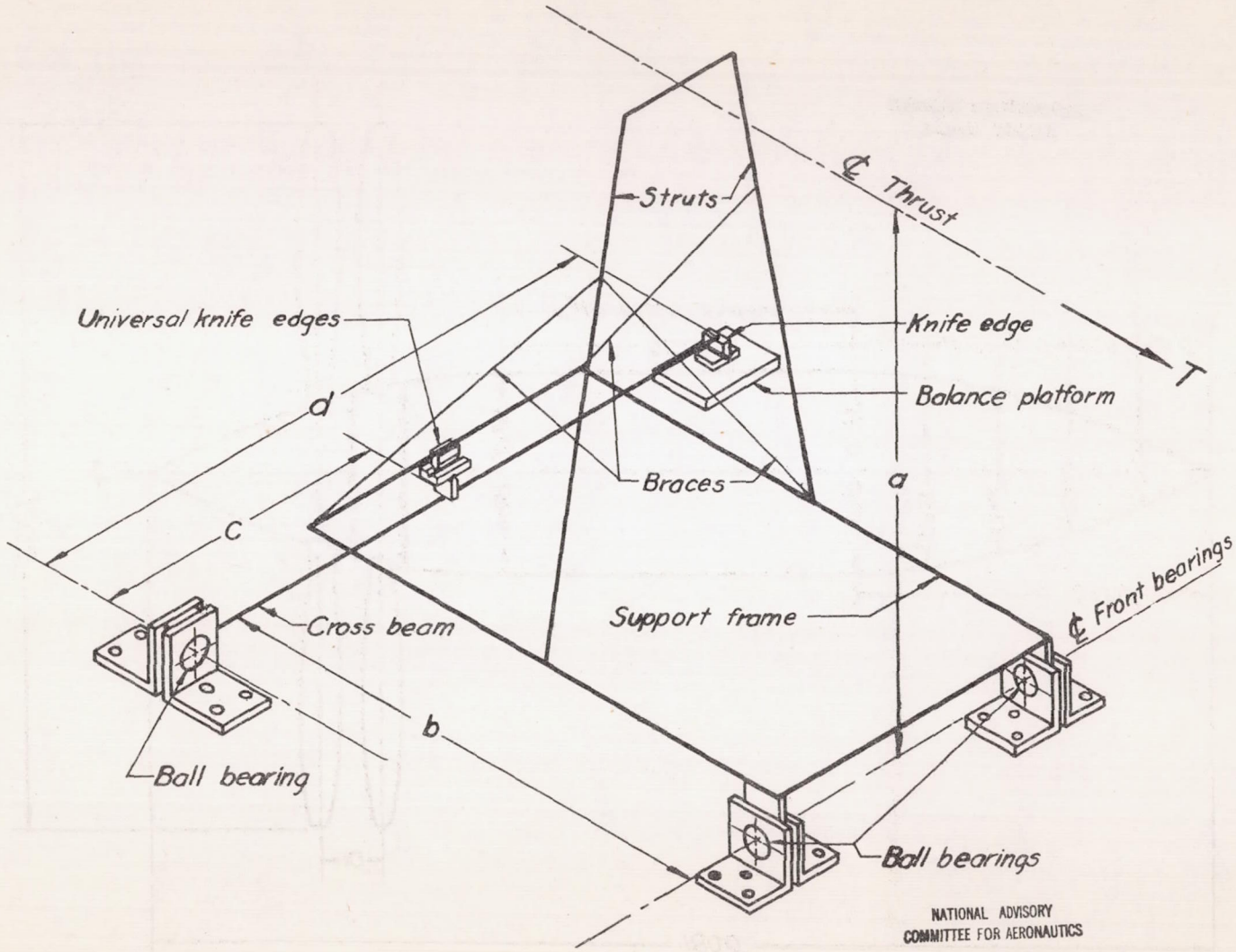


Figure 2.- Diagram of thrust-measuring mechanism.

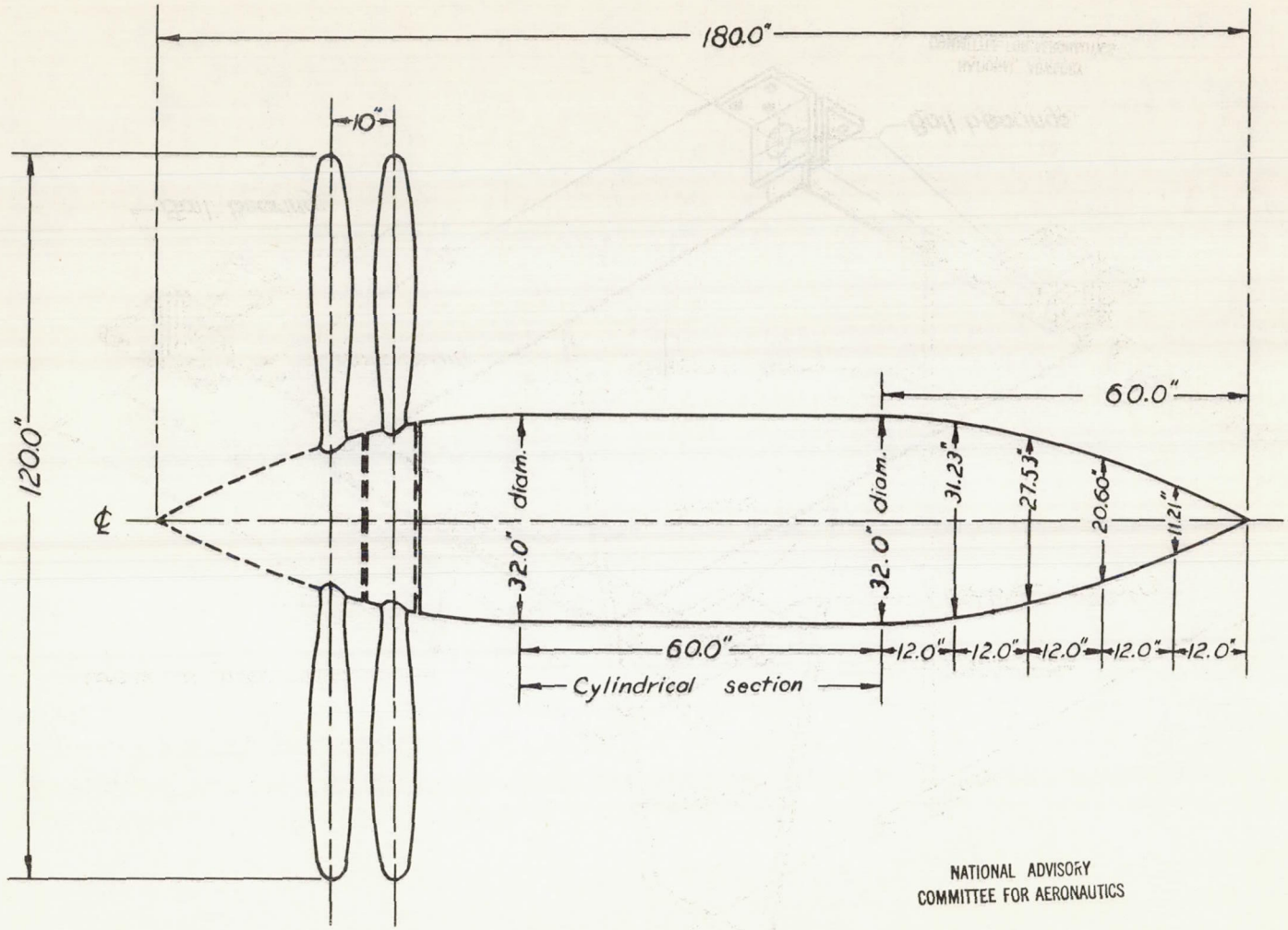


Figure 3.- Plan view showing dimensional details of nacelle.

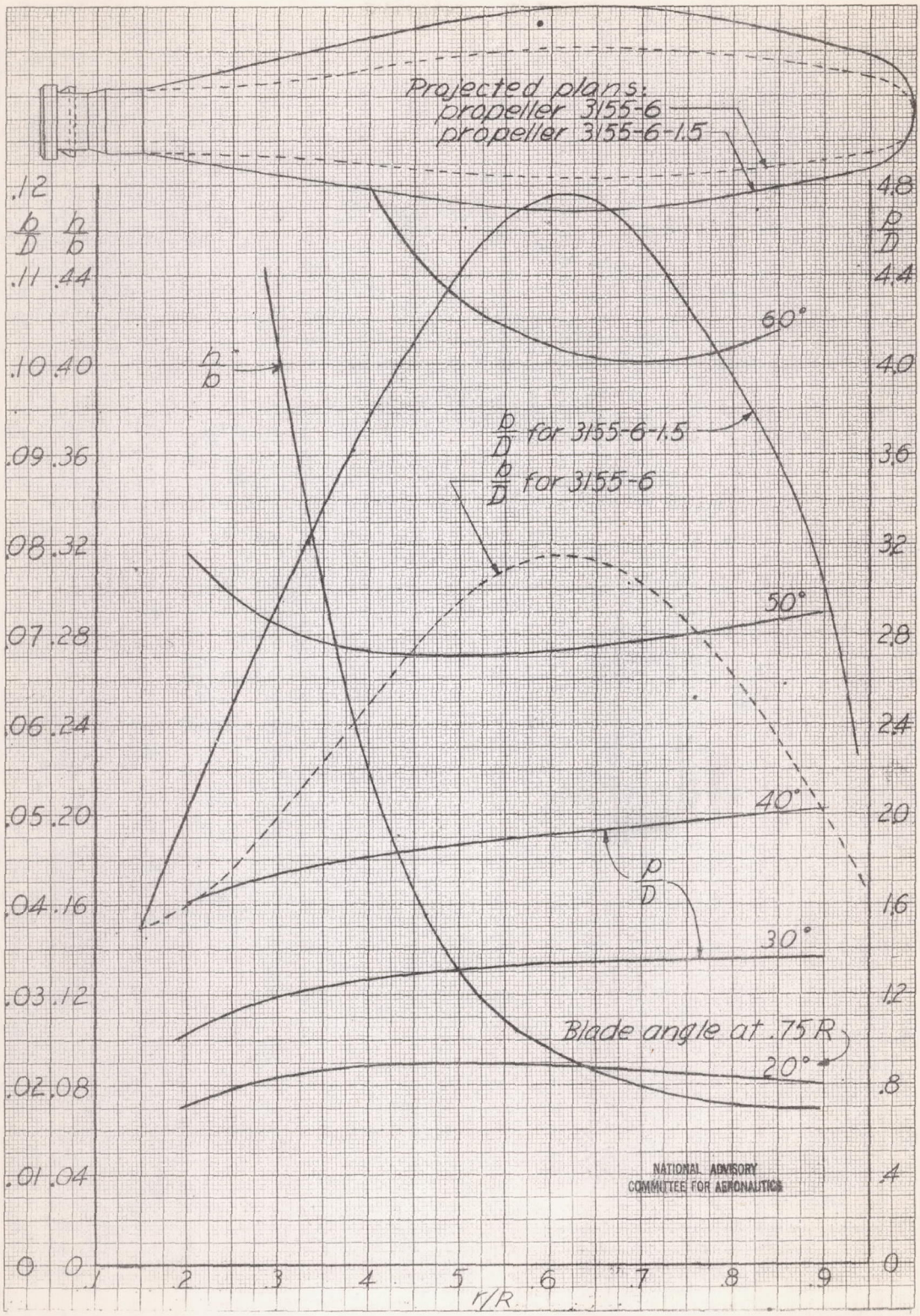


Figure 4.- Blade-form curves, propellers 3155-6 and 3155-6-1.5. Blade-form curves, except b/D, are identical. Symbols are: D, diameter; R, radius; r, station radius: b, section chord; h, section thickness; p, geometric pitch.

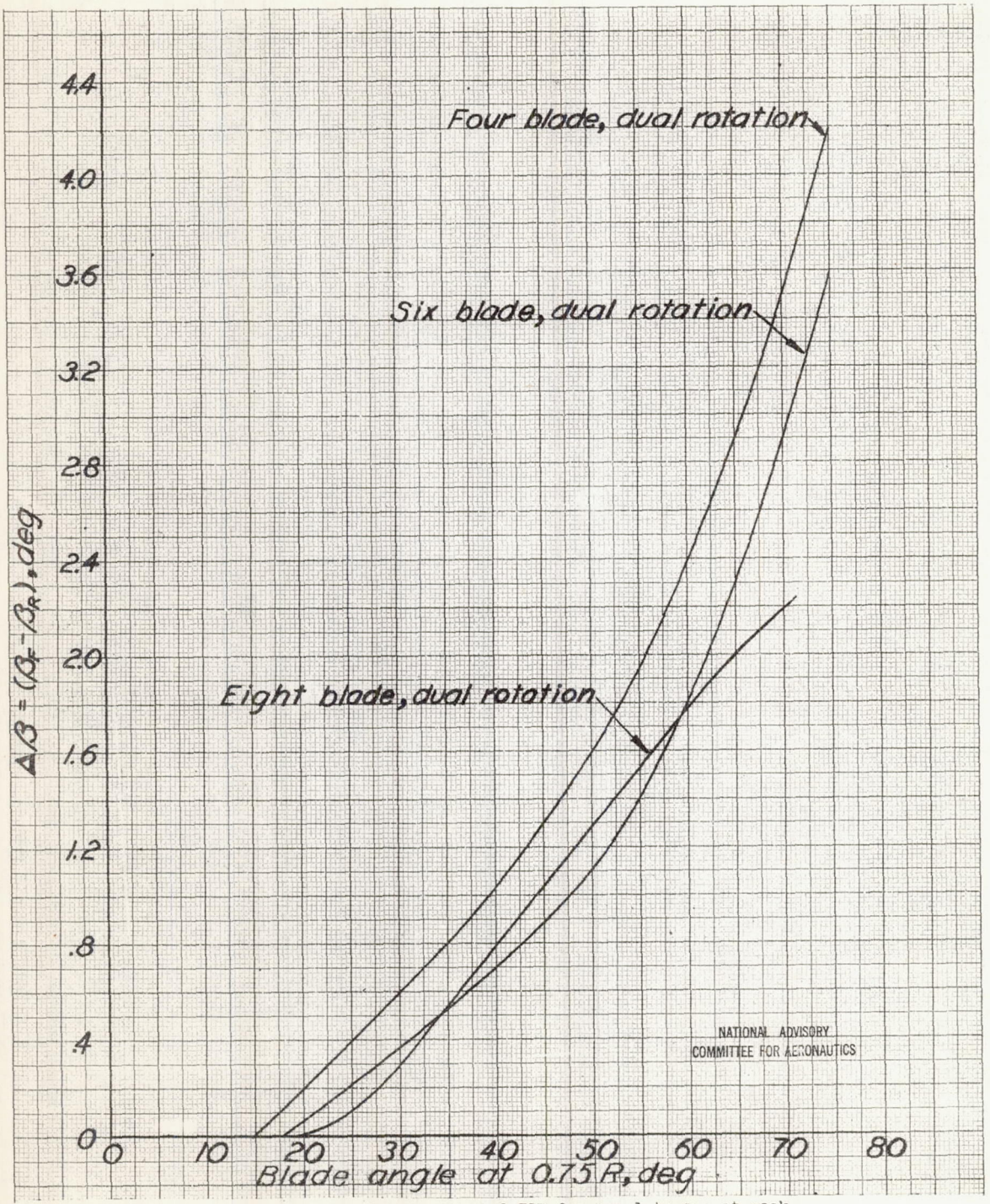
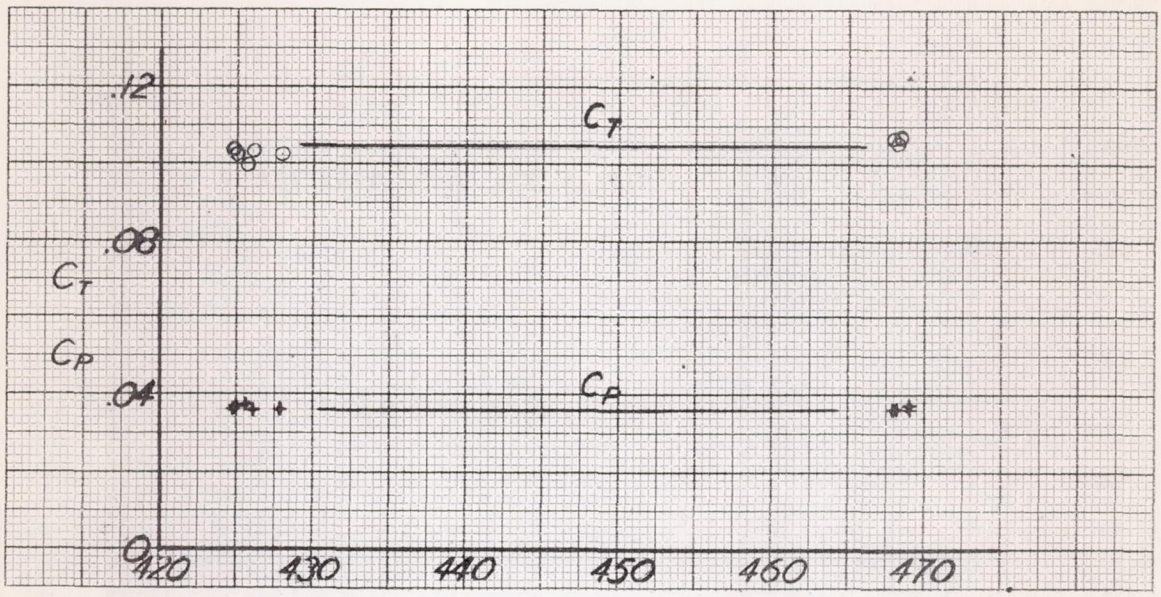
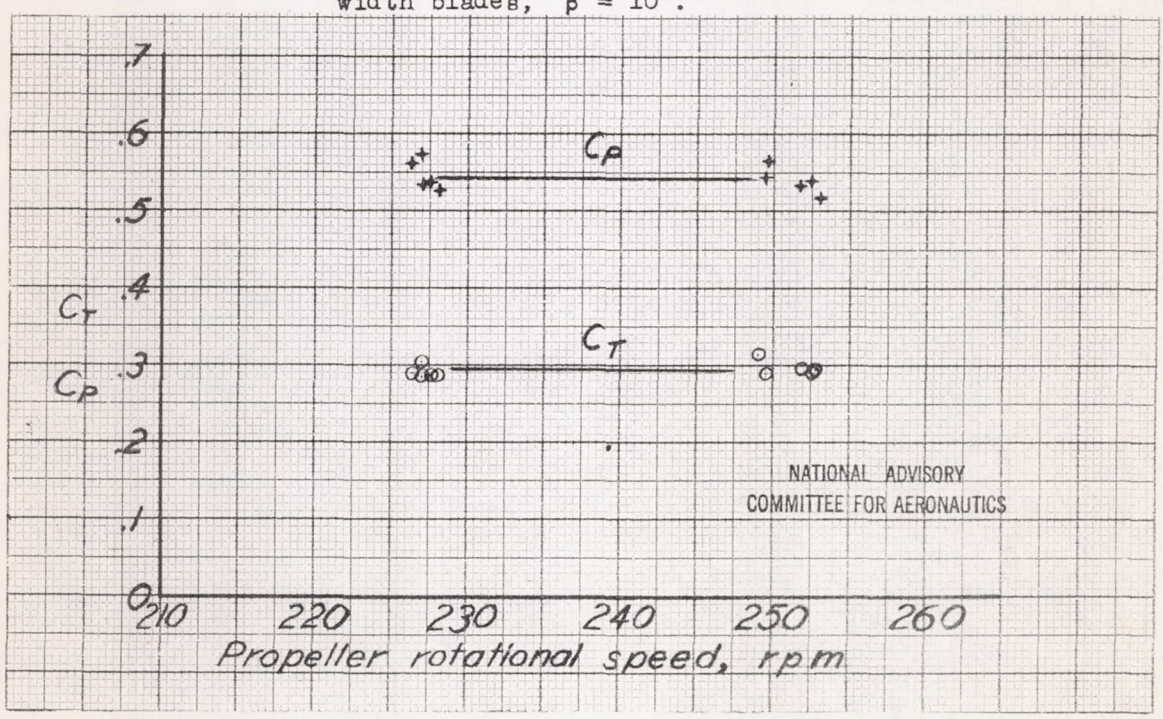


Figure 5.- Difference in blade angle at 0.75R for equal torque at peak efficiency.



(a) Three-blade single-rotating propeller, standard-width blades, $\beta = 10^\circ$.



(b) Six-blade single-rotating propeller, standard width blades, $\beta = 40^\circ$.

Figure 6.- Typical initial test results uncorrected for wind velocity.

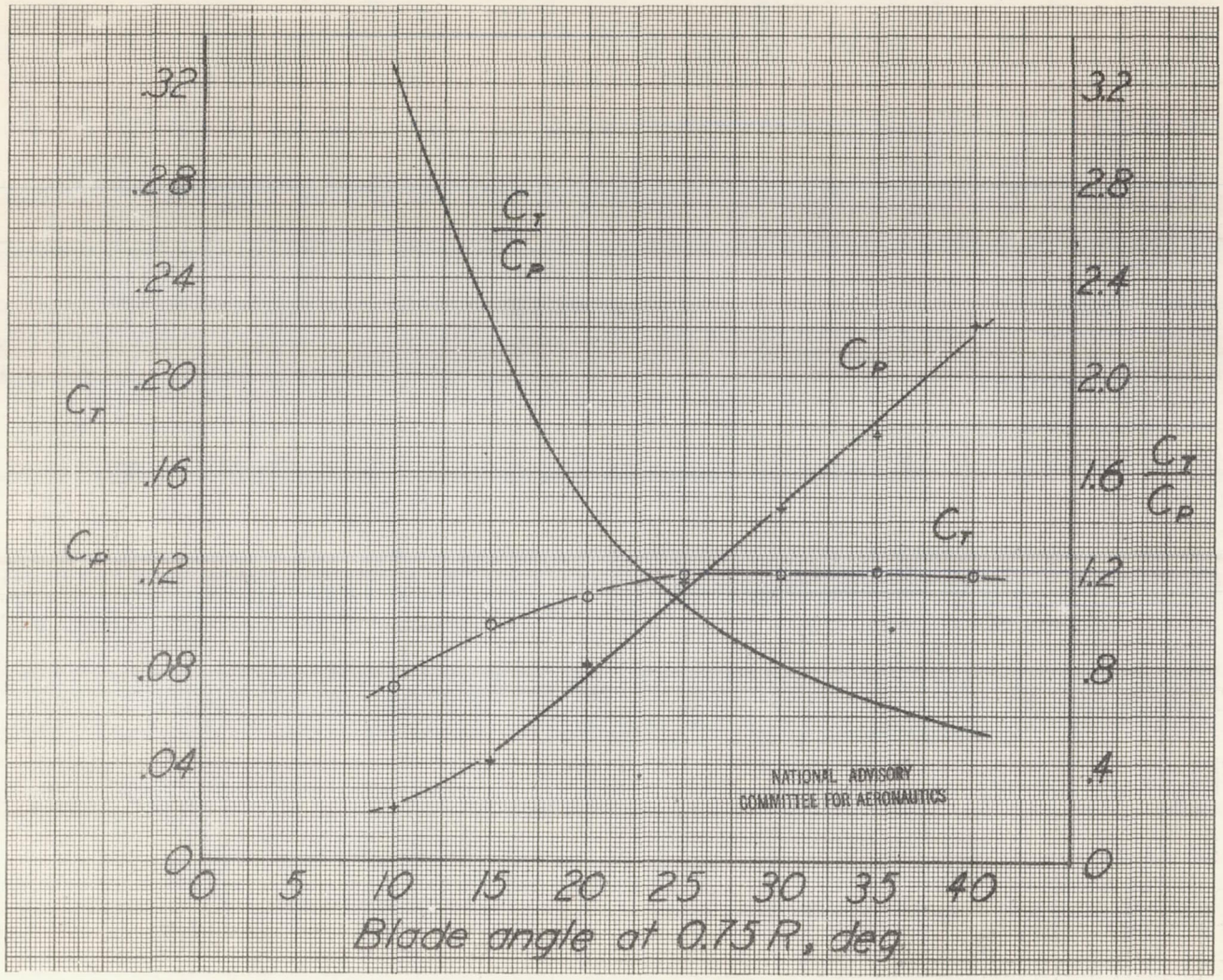


Figure 7.- Static characteristics of two-blade single-rotating propeller. Standard-width blades.

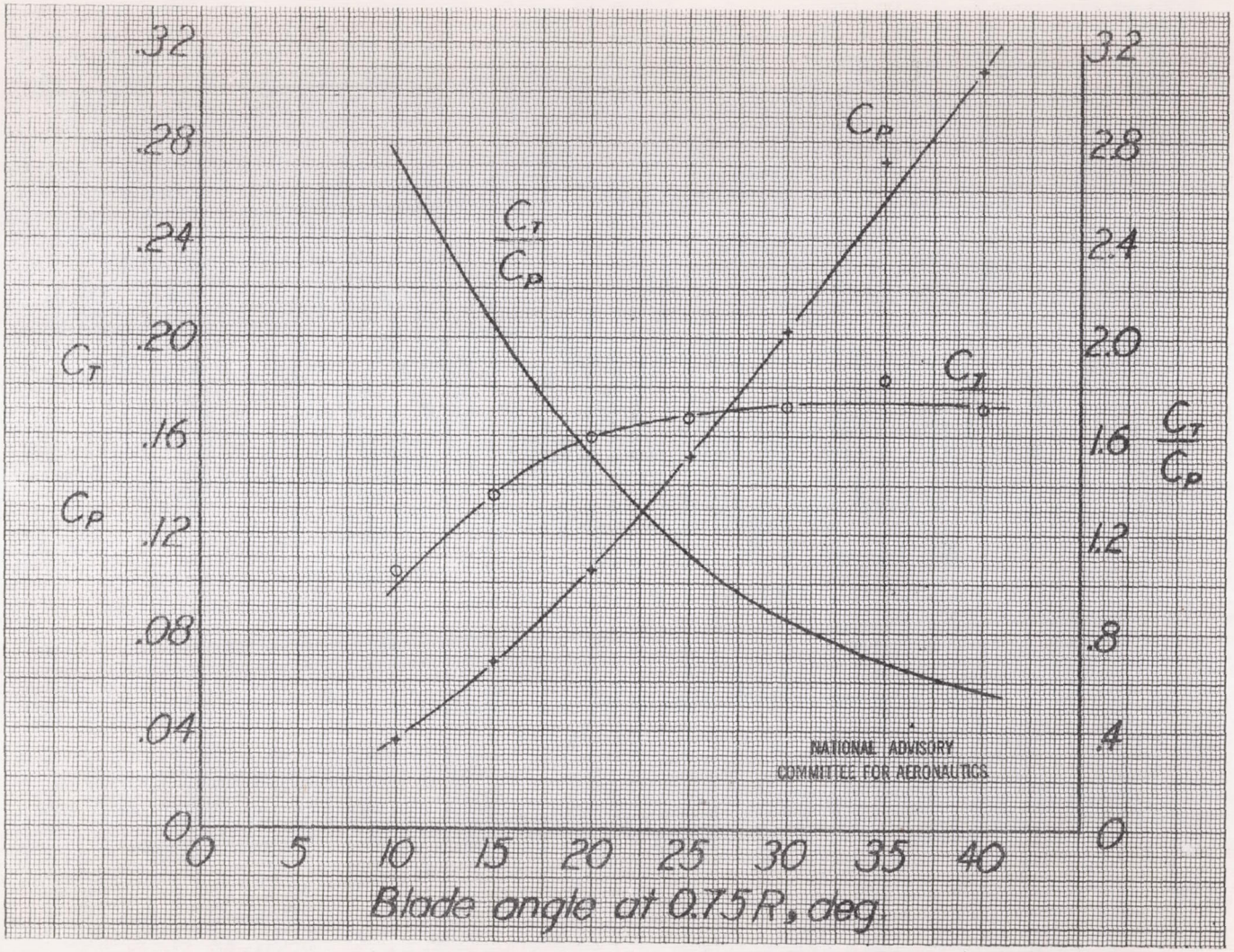


Figure 8.- Static characteristics of three-blade single-rotating propeller. Standard width blades.

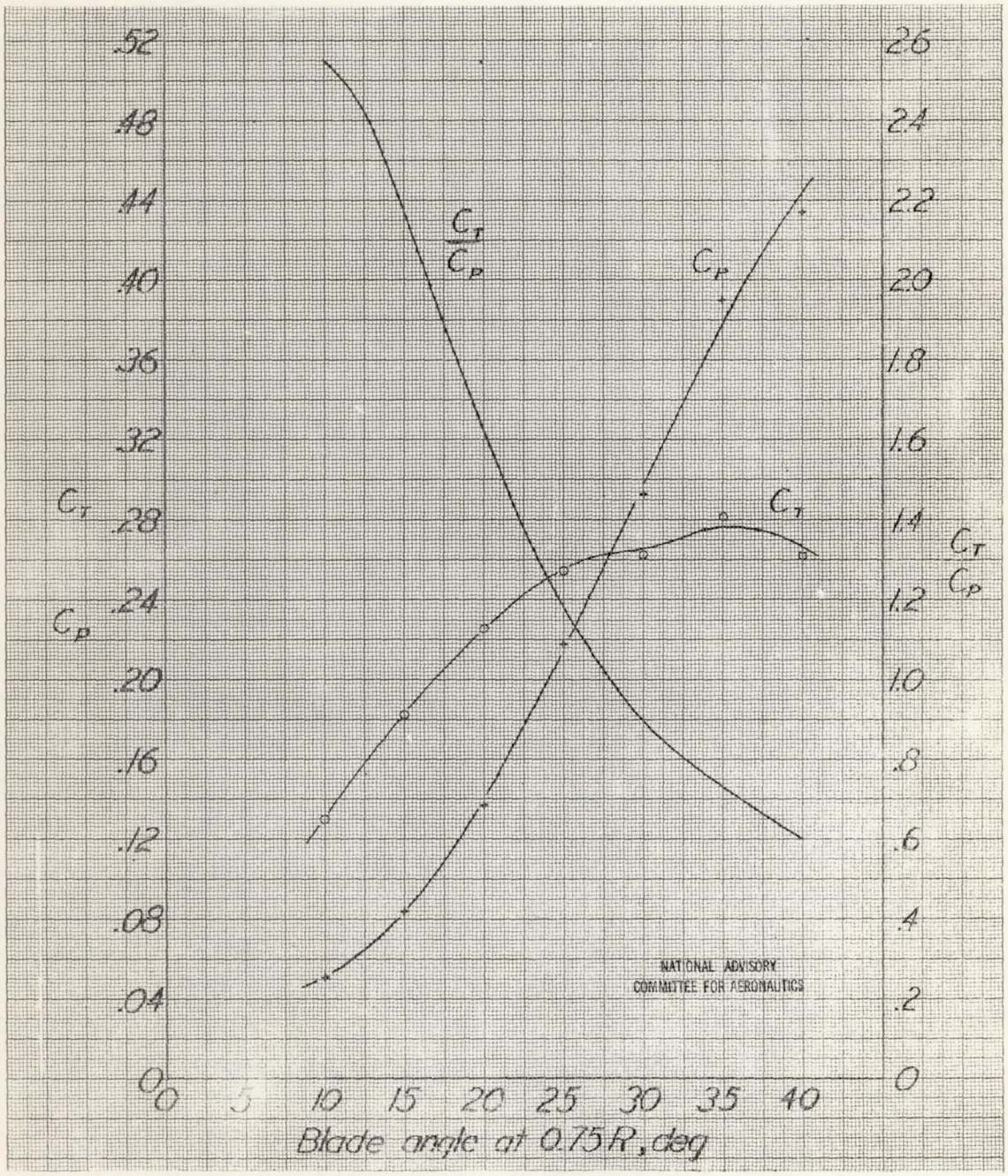


Figure 9.- Static characteristics of three-blade single-rotating propeller. Wide blades.

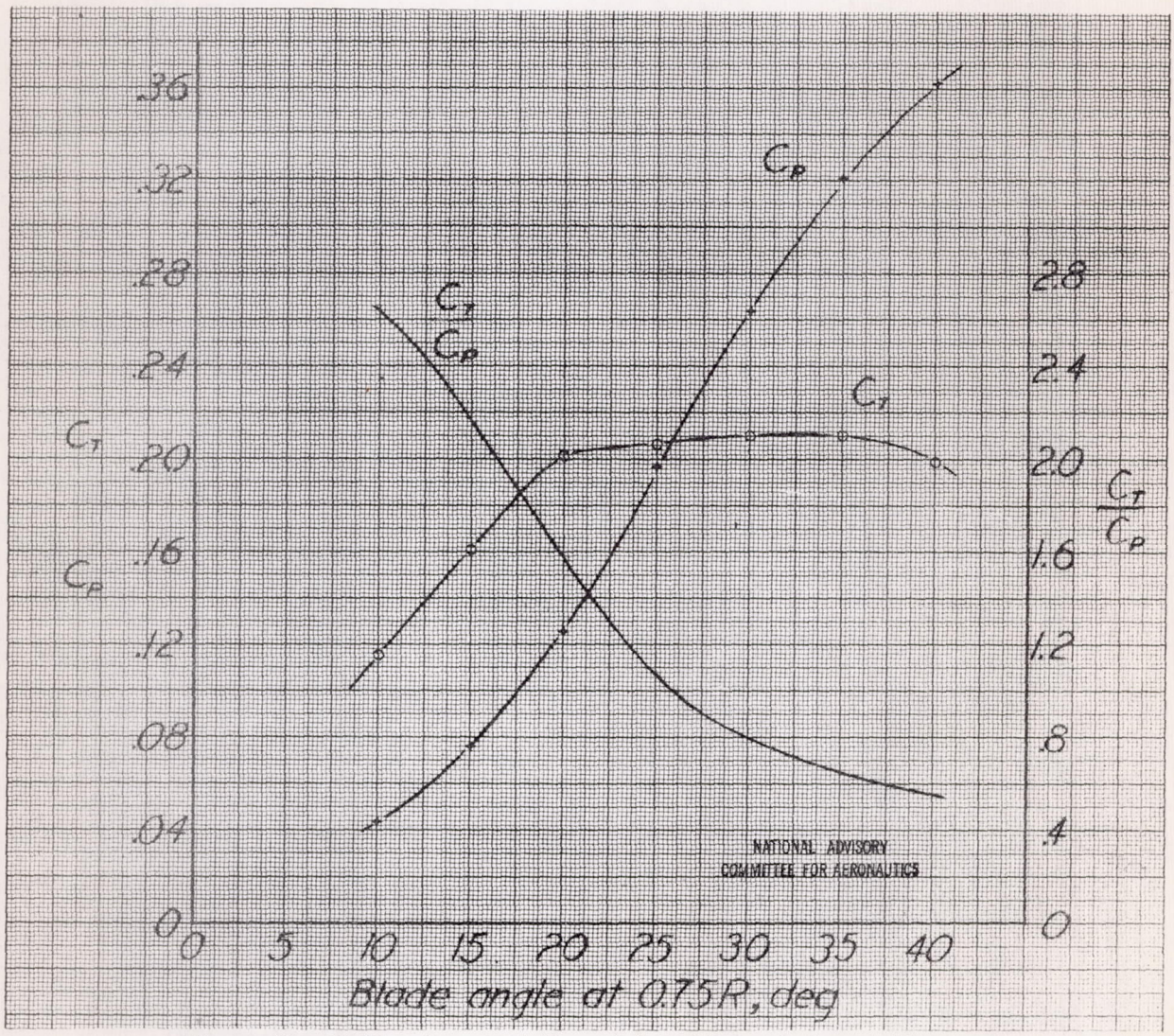


Figure 10.- Static characteristics of four-blade single-rotating propeller. Standard-width blades.

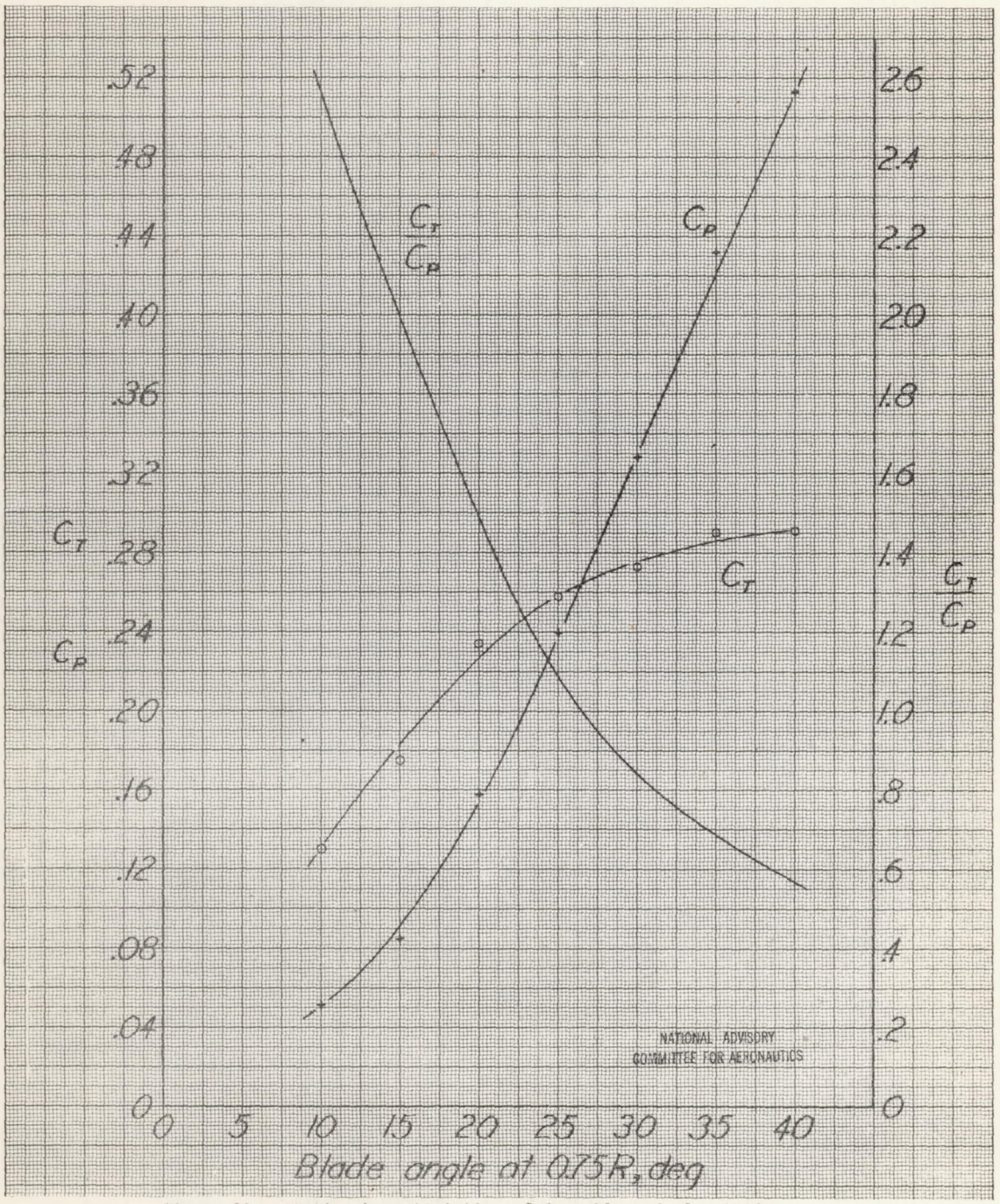


Figure 11.- Static characteristics of four-blade dual-rotating propeller. Standard-width blades.

L-750

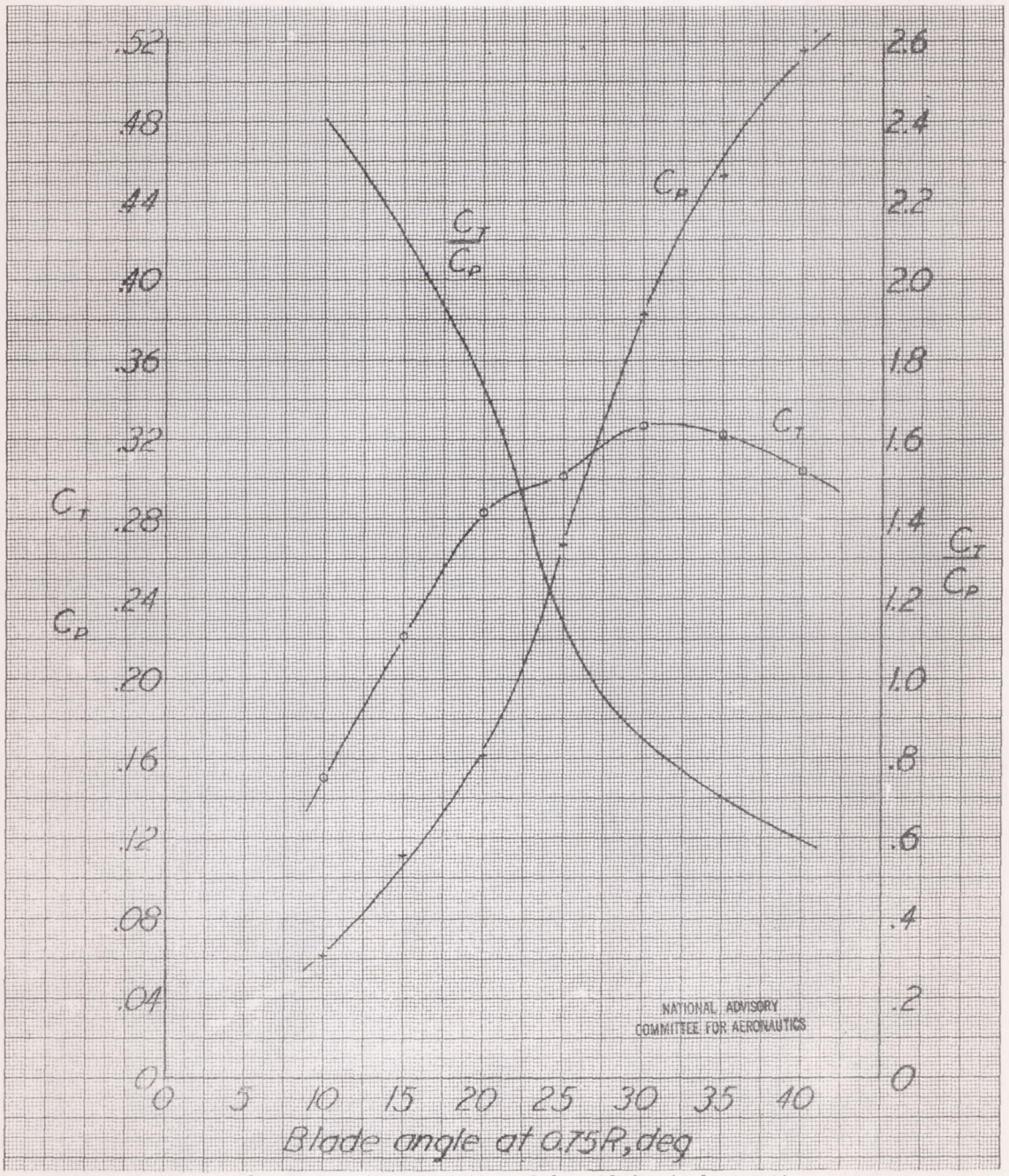


Figure 12.- Static characteristics of four-blade single-rotating propeller. Wide blades.

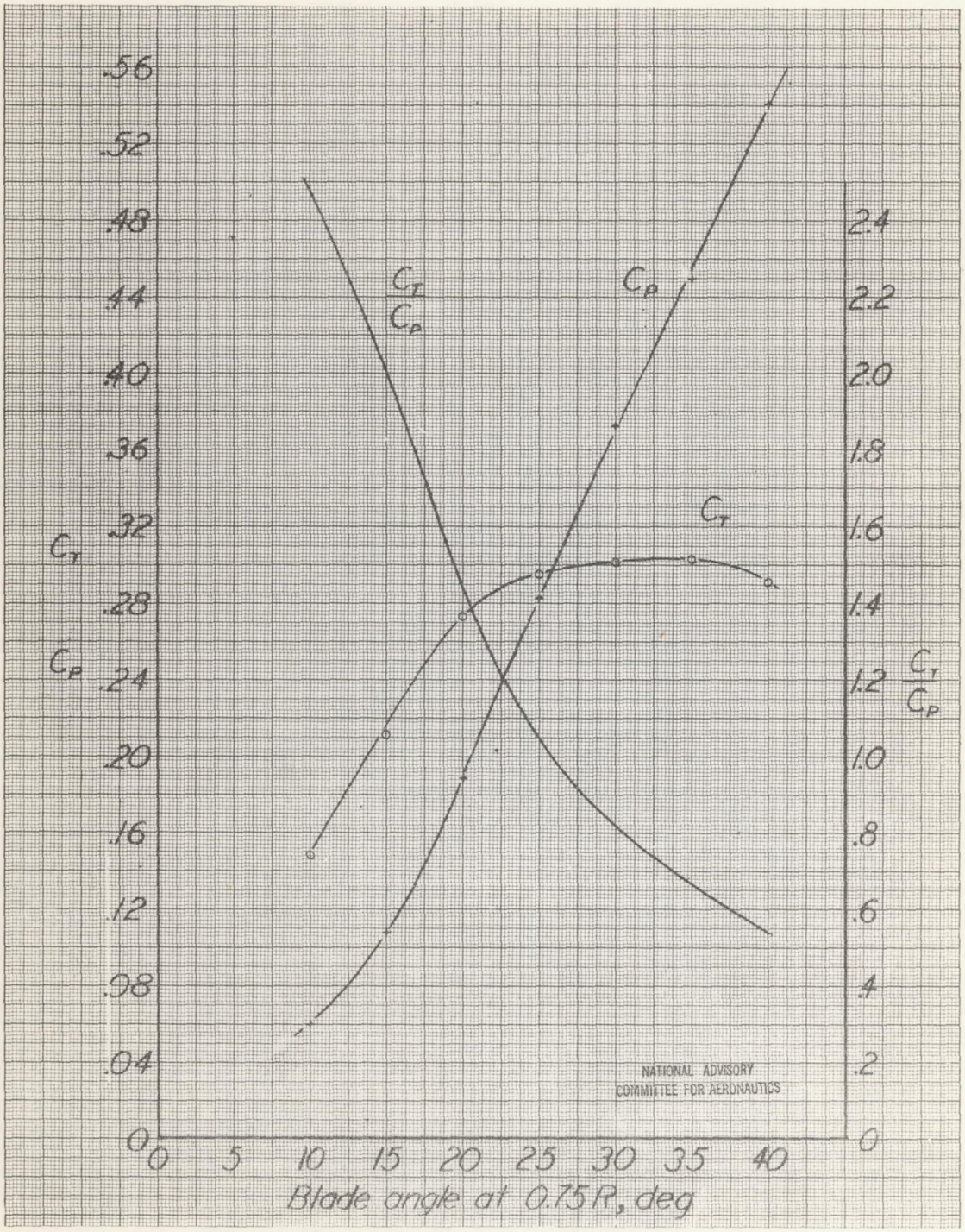


Figure 13.- Static characteristics of six-blade single-rotating propeller. Standard-width blades.

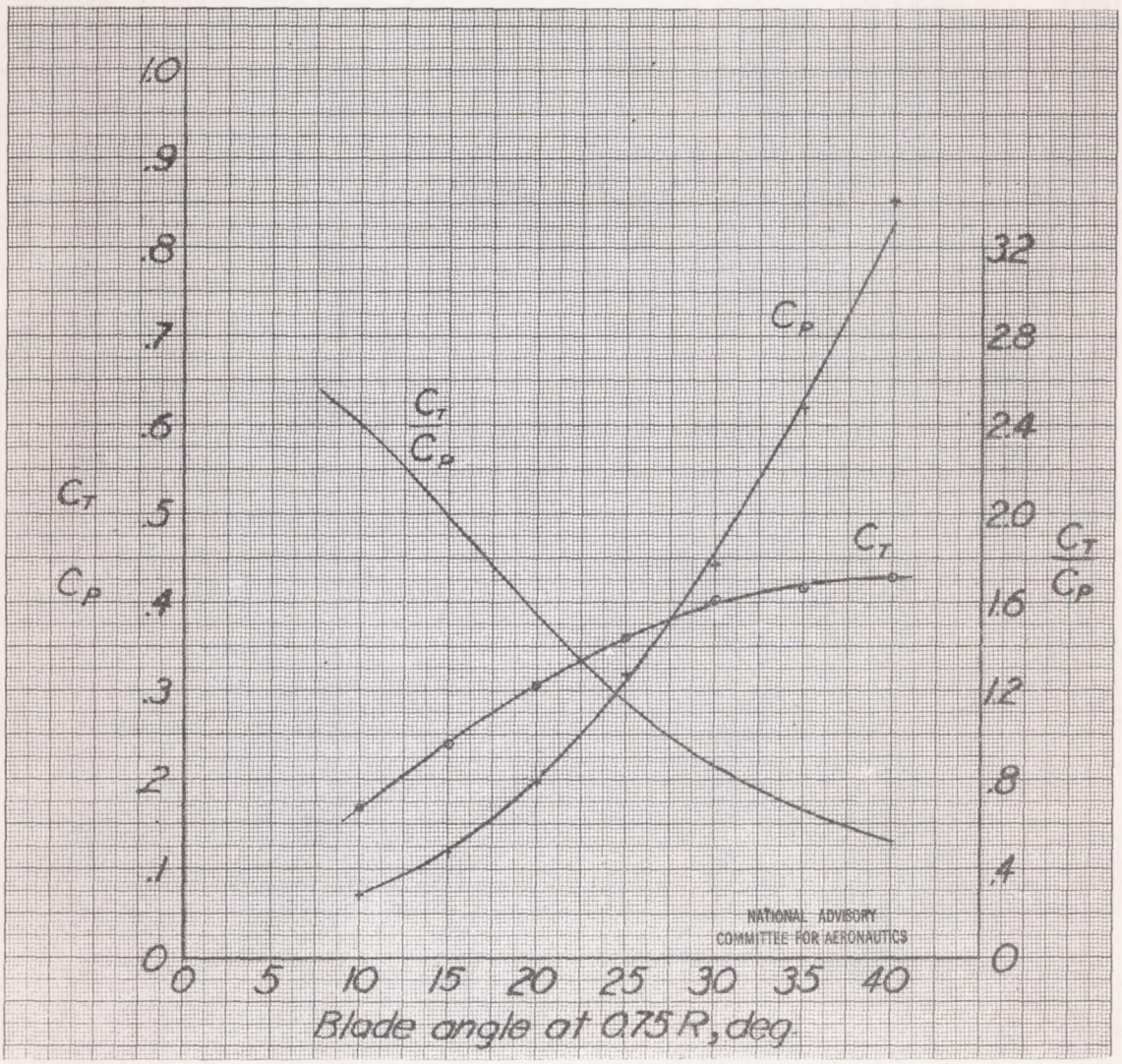


Figure 14.- Static characteristics of six-blade dual-rotating propeller. Standard-width blades.

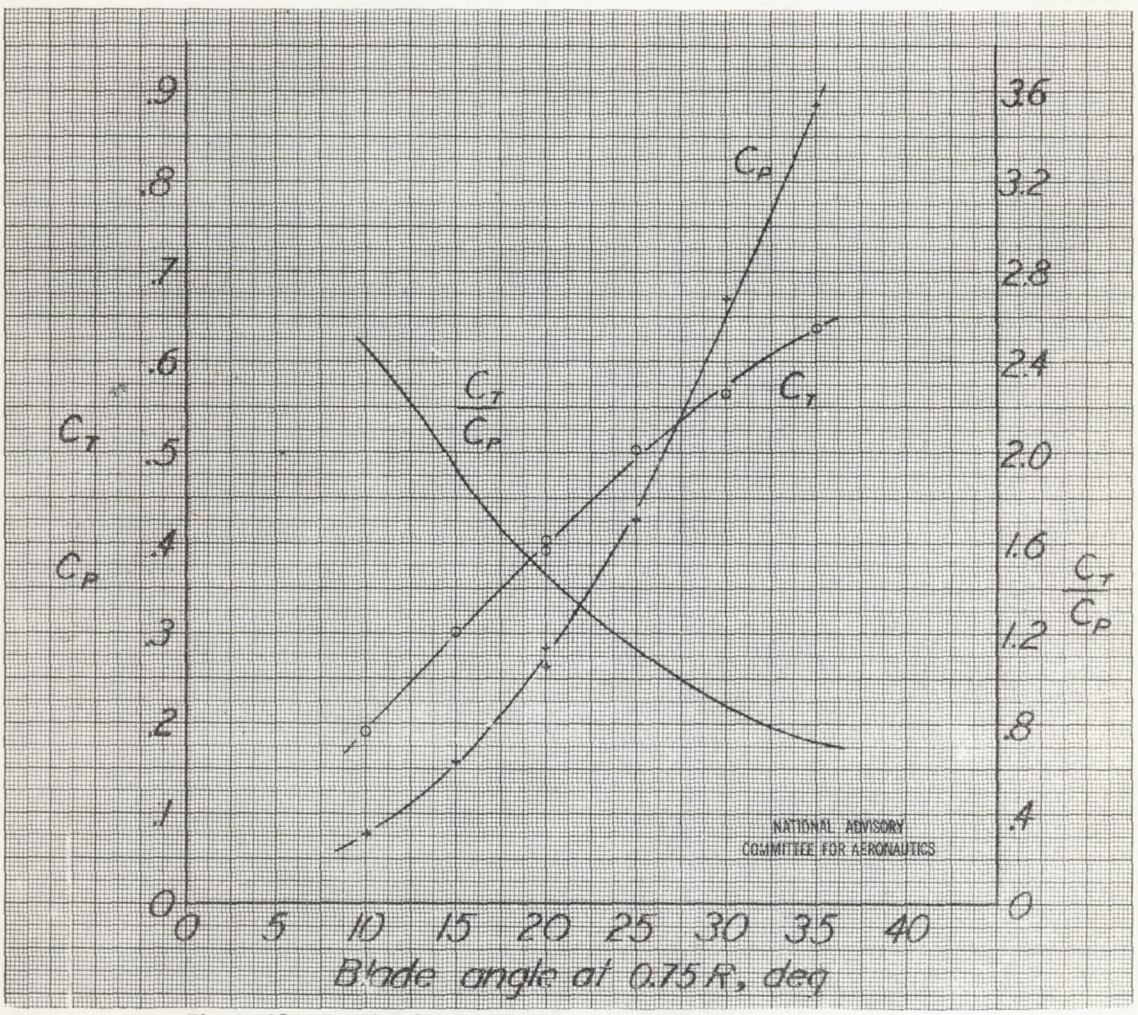


Figure 15.- Static characteristics of six-blade dual-rotating propeller. Wide blades.

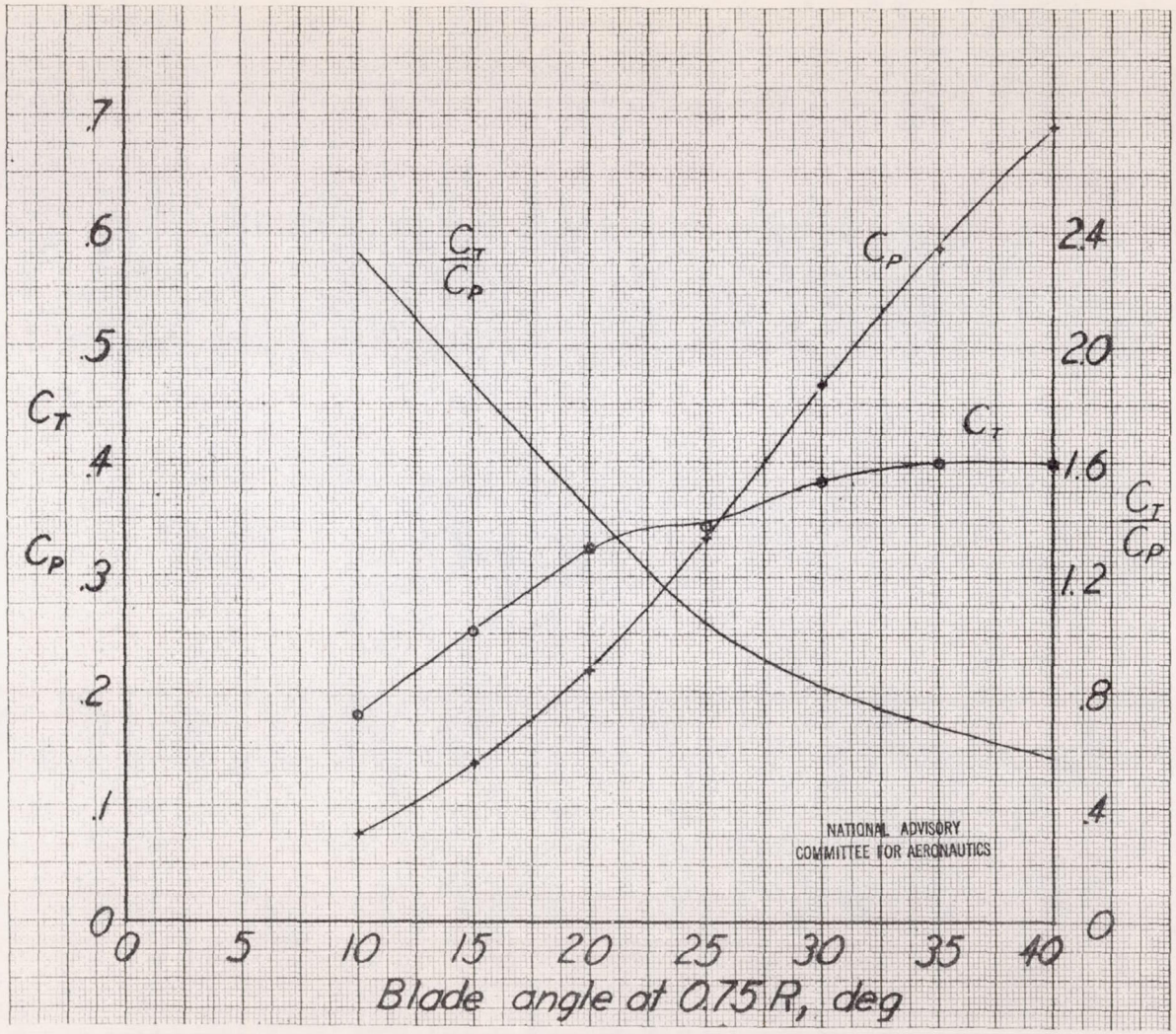


Figure 16.- Static characteristics of eight-blade single-rotating propeller. Standard-width blades.

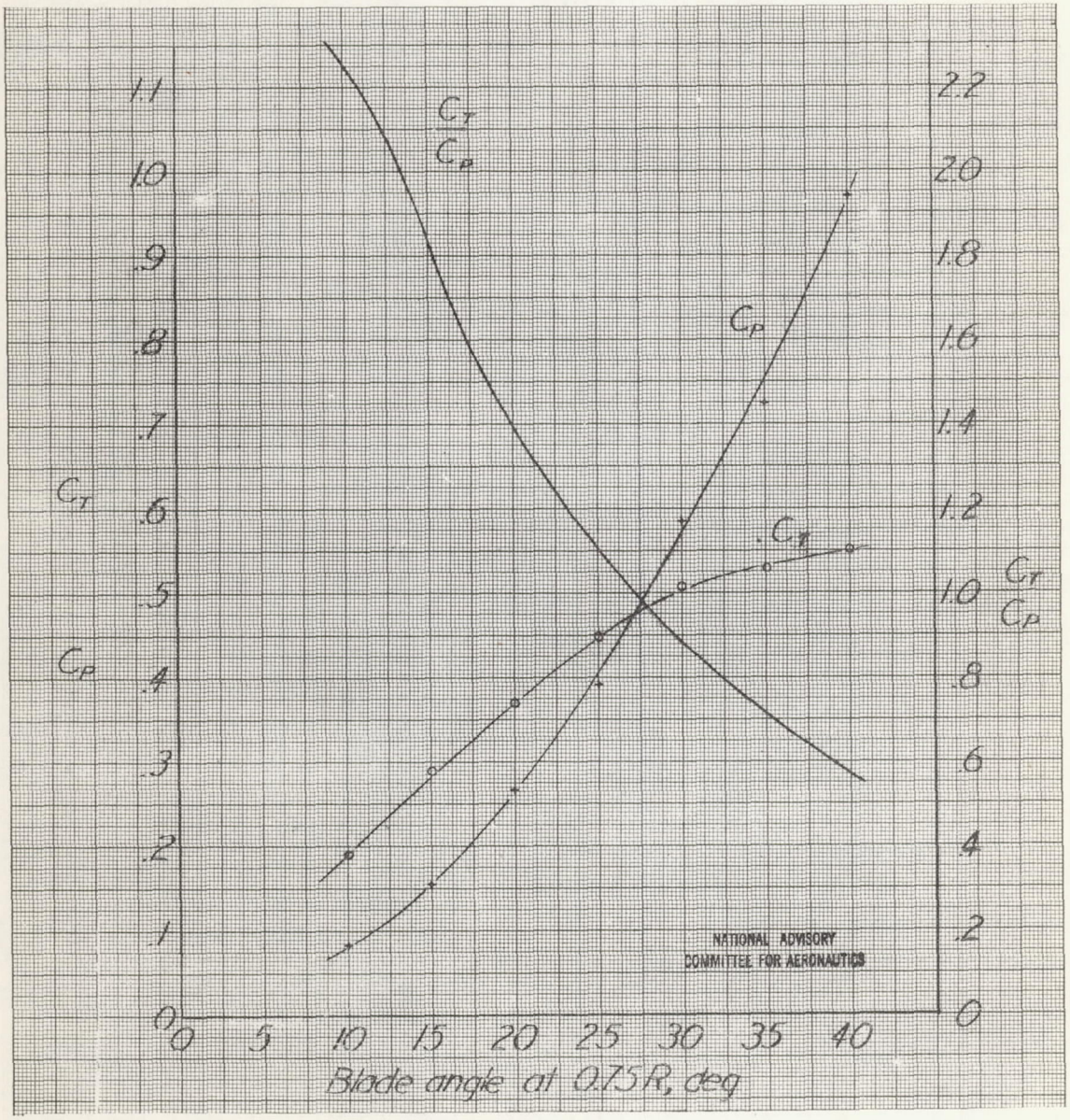


Figure 17.- Static characteristics of eight-blade dual-rotating propeller. Standard-width blades.

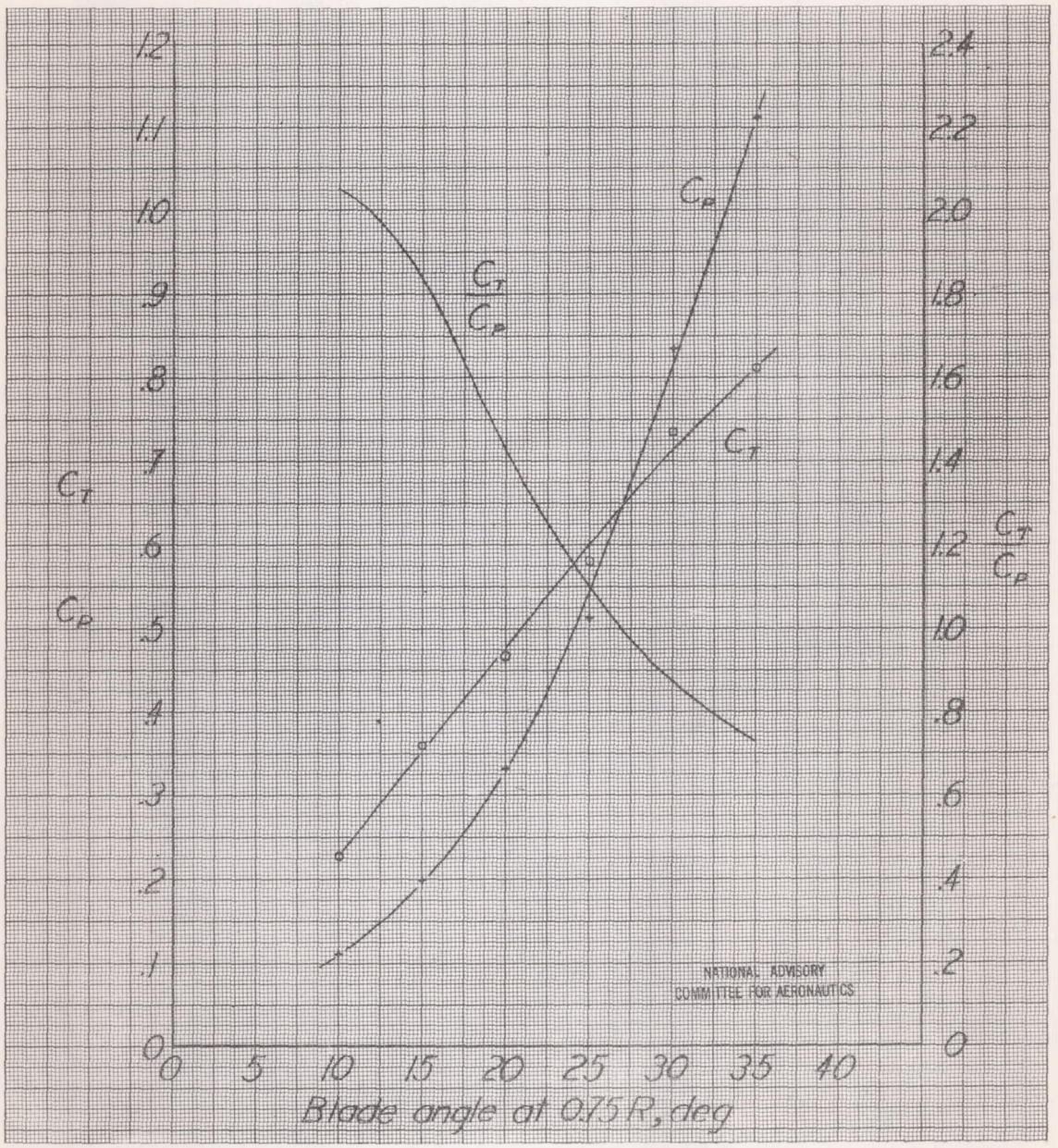


Figure 18.- Static characteristics of eight-blade dual-rotating propeller. Wide blades.

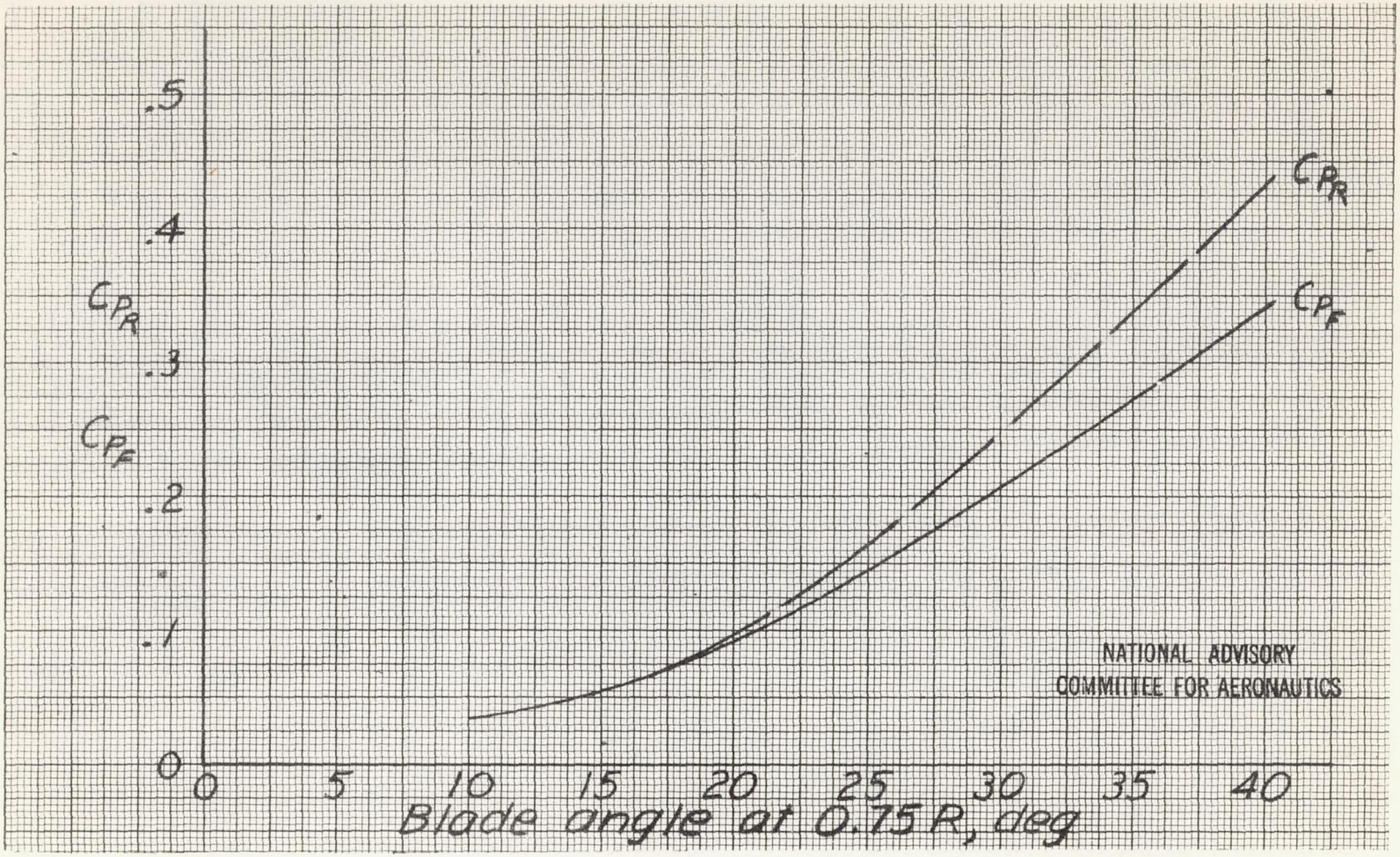


Figure 19.- Variation of the power absorption of the front and rear components of the six-blade dual-rotating propeller. Standard-width blades.

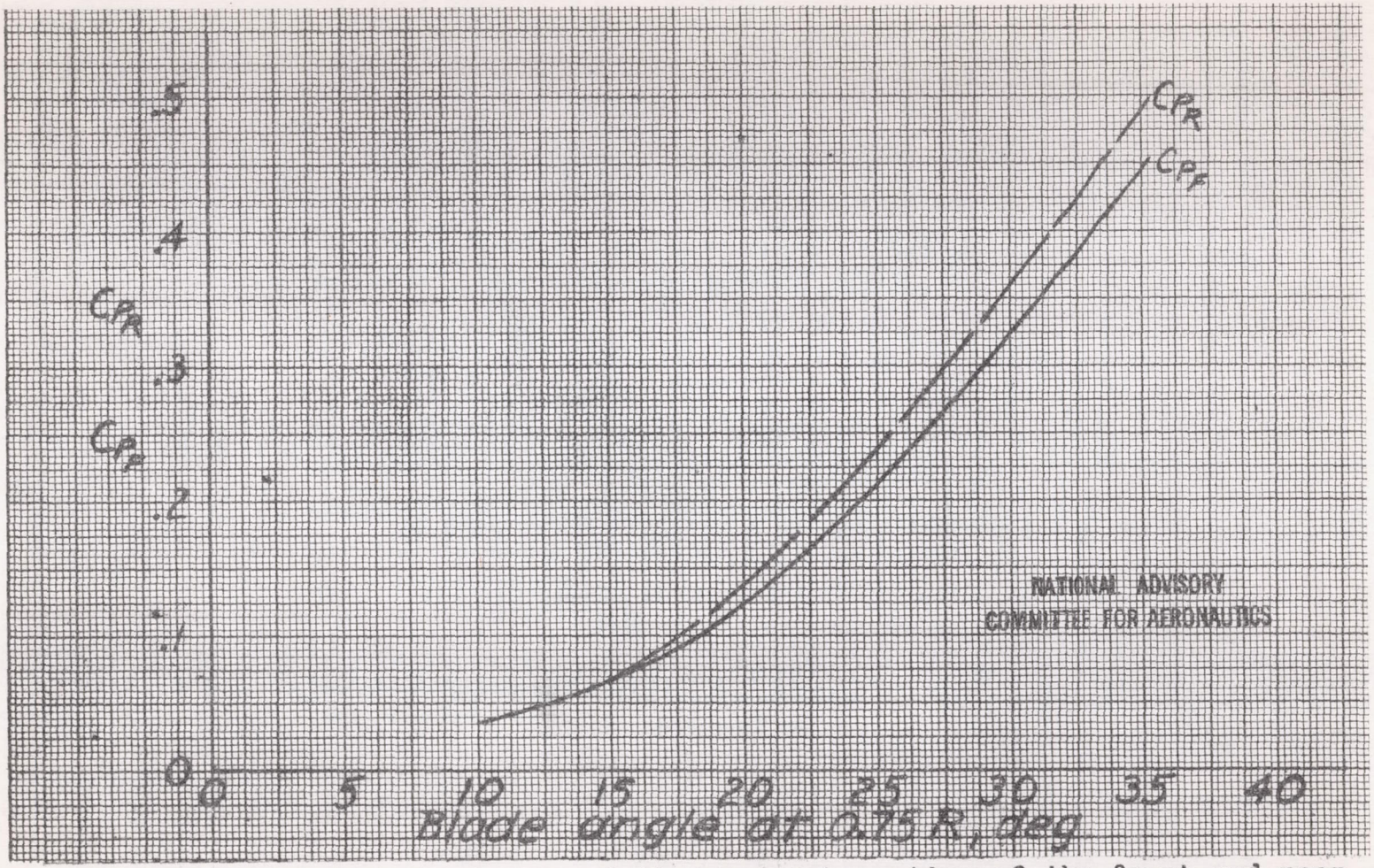
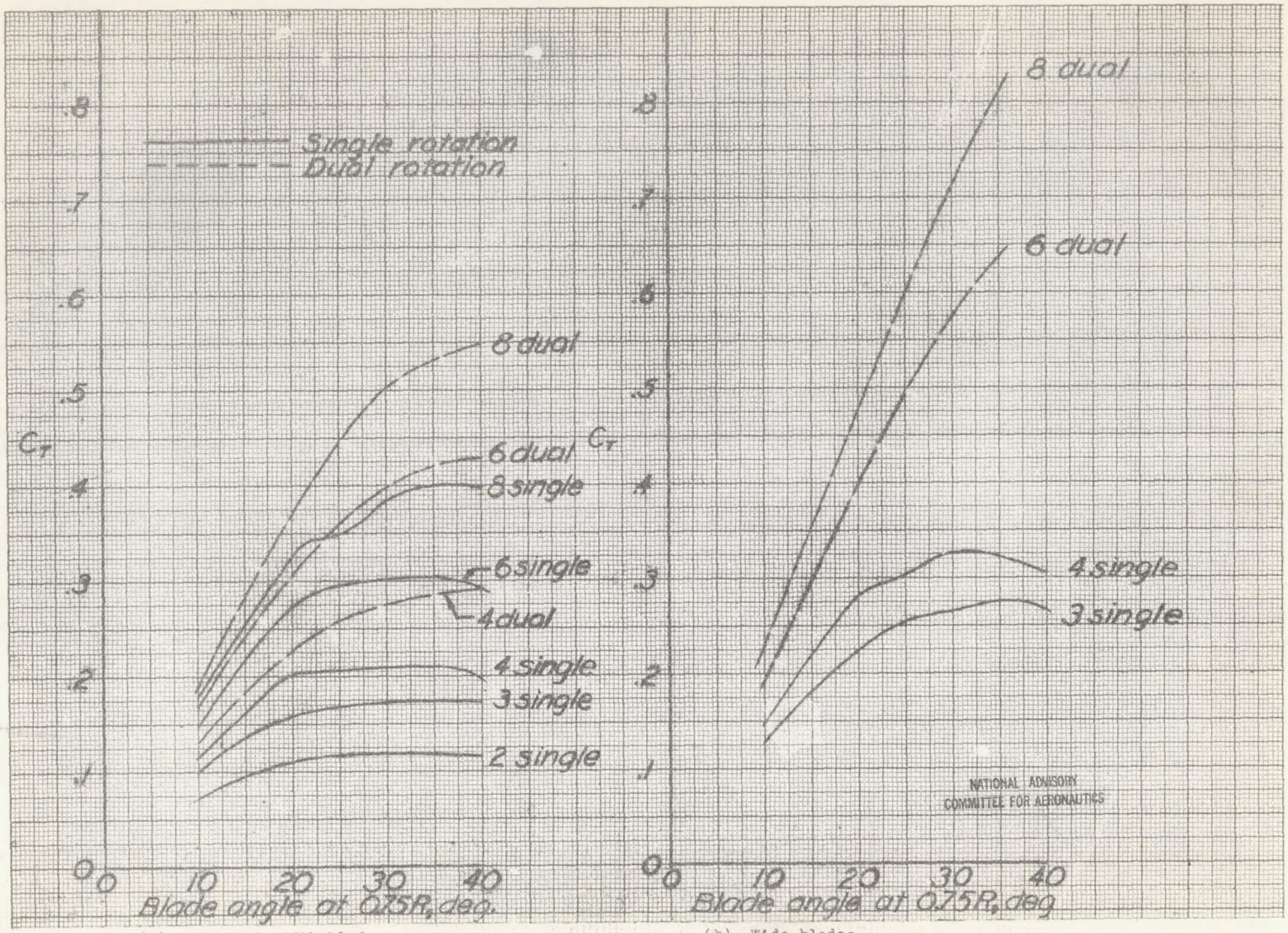


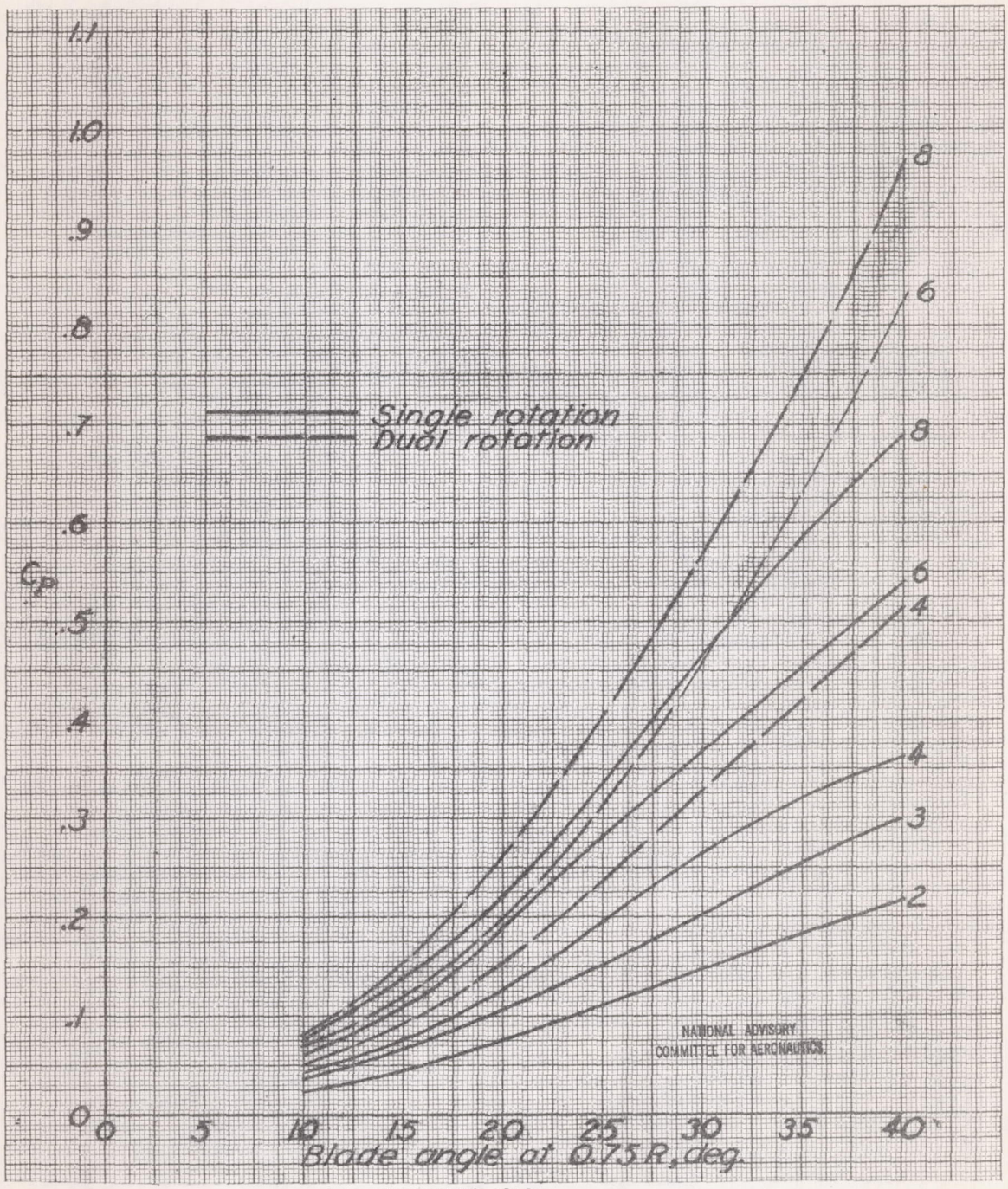
Figure 20.- Variation of the power absorption of the front and rear components of the six-blade dual-rotating propeller. Wide blades.



(a) Standard-width blades.

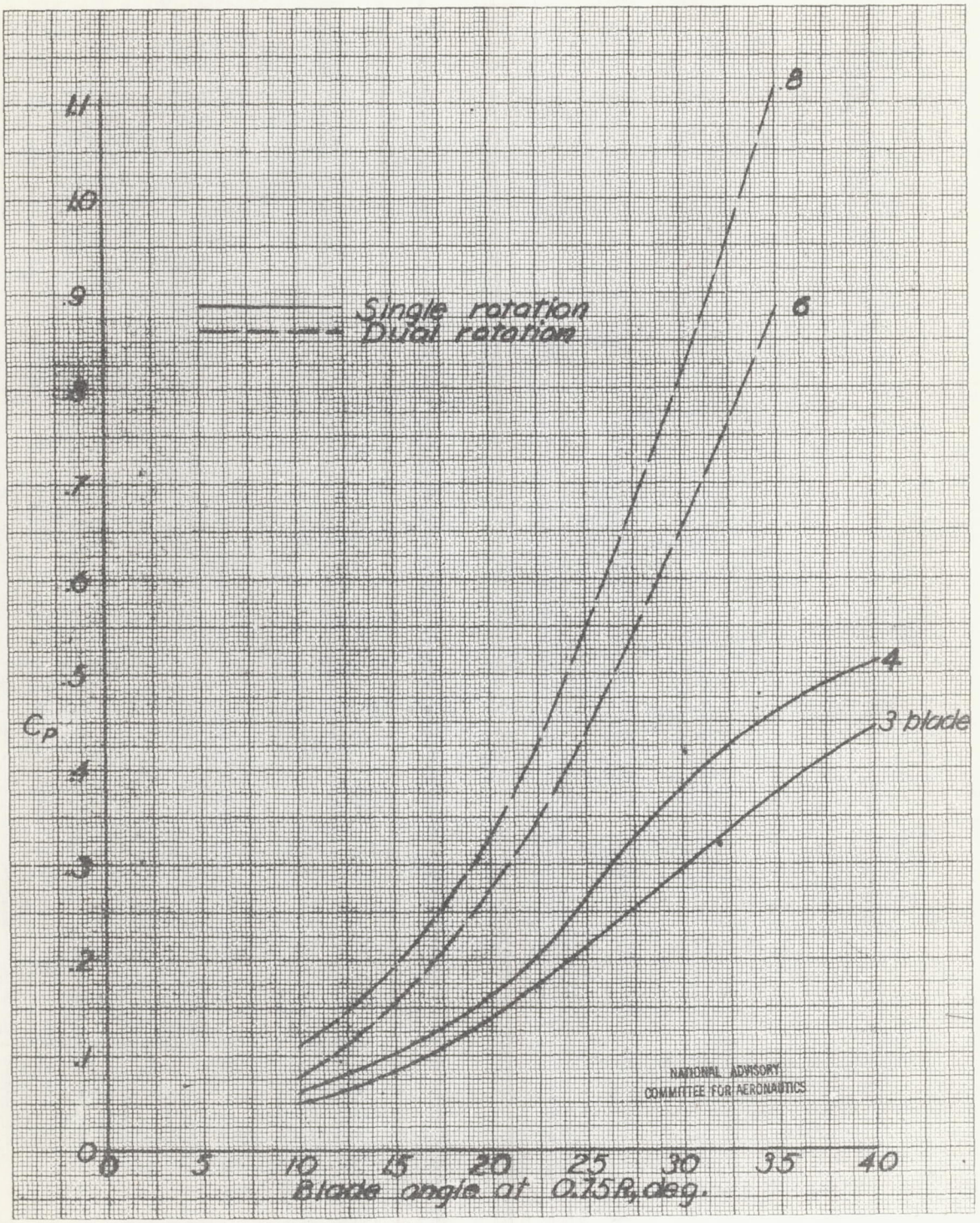
(b) Wide blades.

Figure 21.- Composite of static-thrust coefficient curves.



(a) Standard-width blades.

Figure 22.- Composite of static-power coefficient curves.



(b) Wide blades.

Figure 22.- Concluded

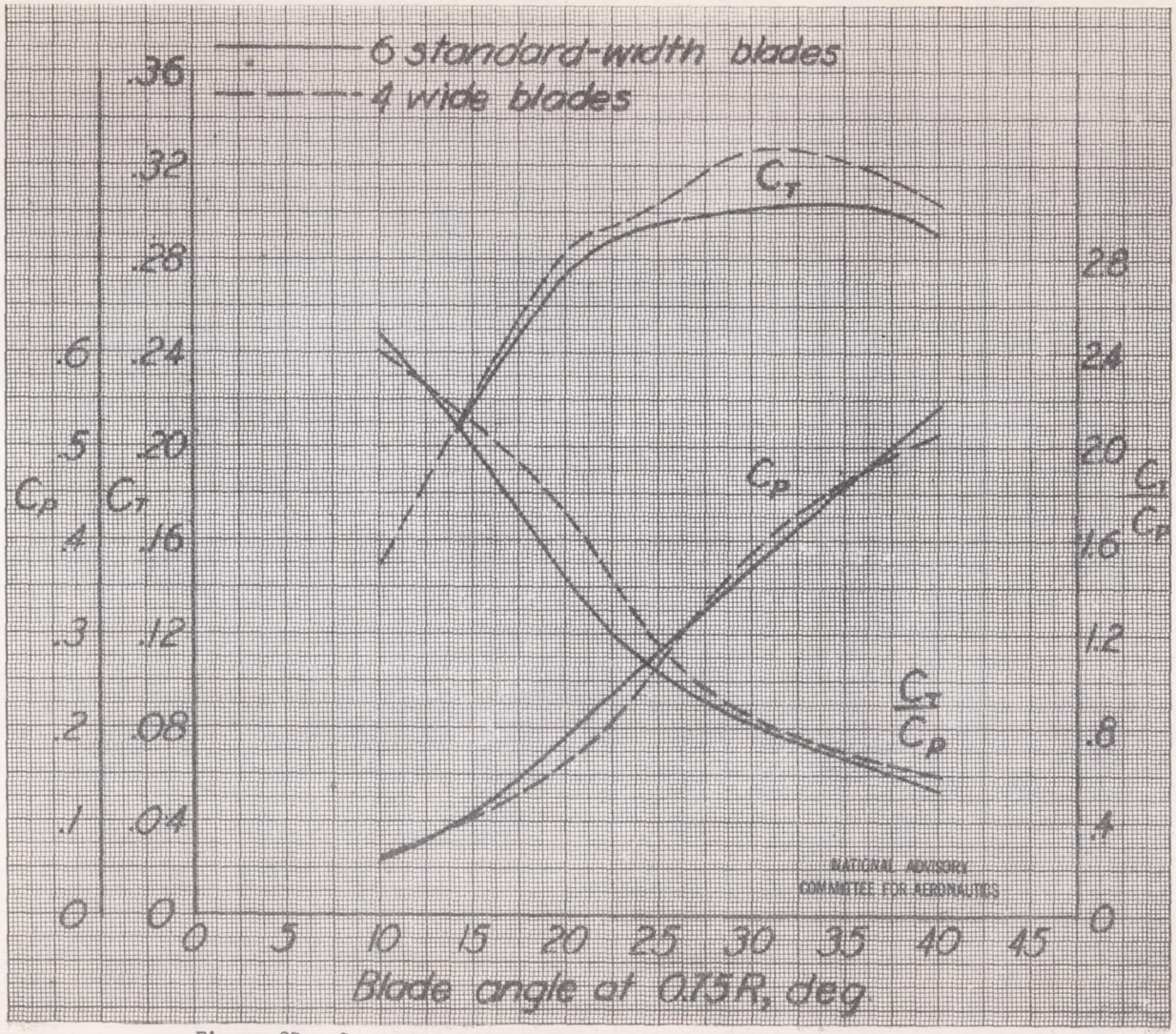


Figure 23.- Comparison of single-rotating propellers of equal solidity. Six standard-width and four wide blades.

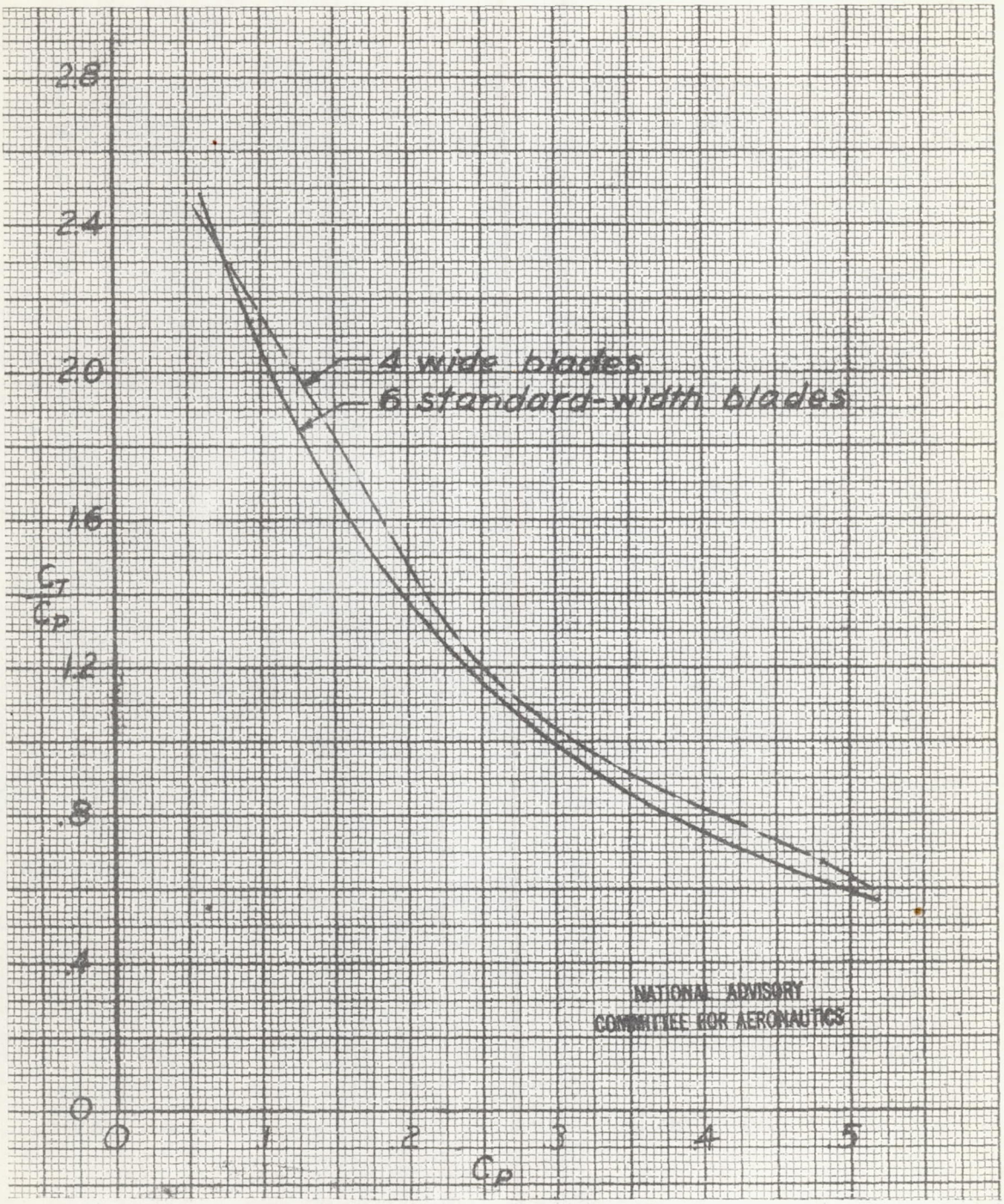


Figure 24.- Comparison of single-rotating propellers of equal solidity on equal power basis.

L-750

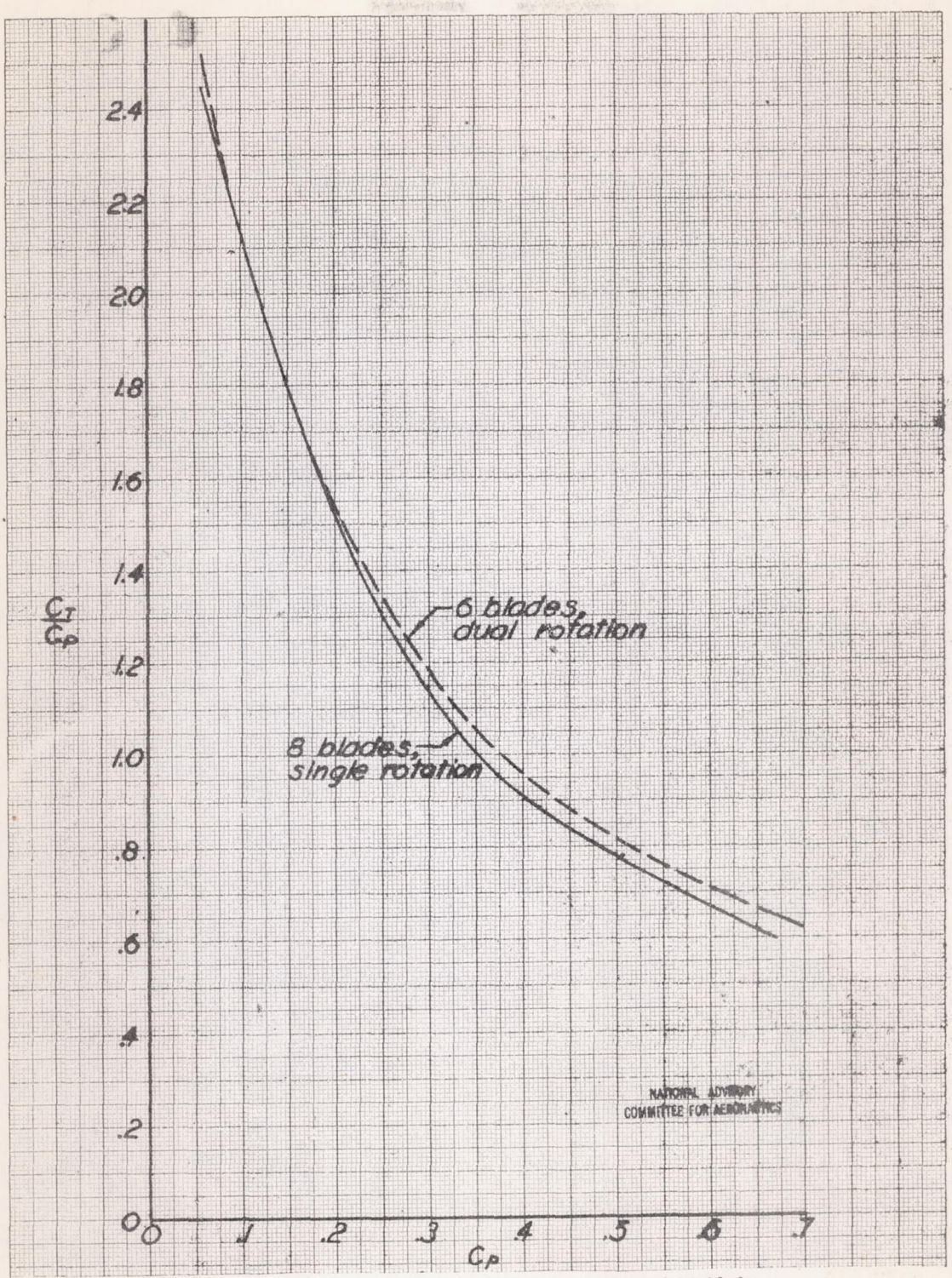
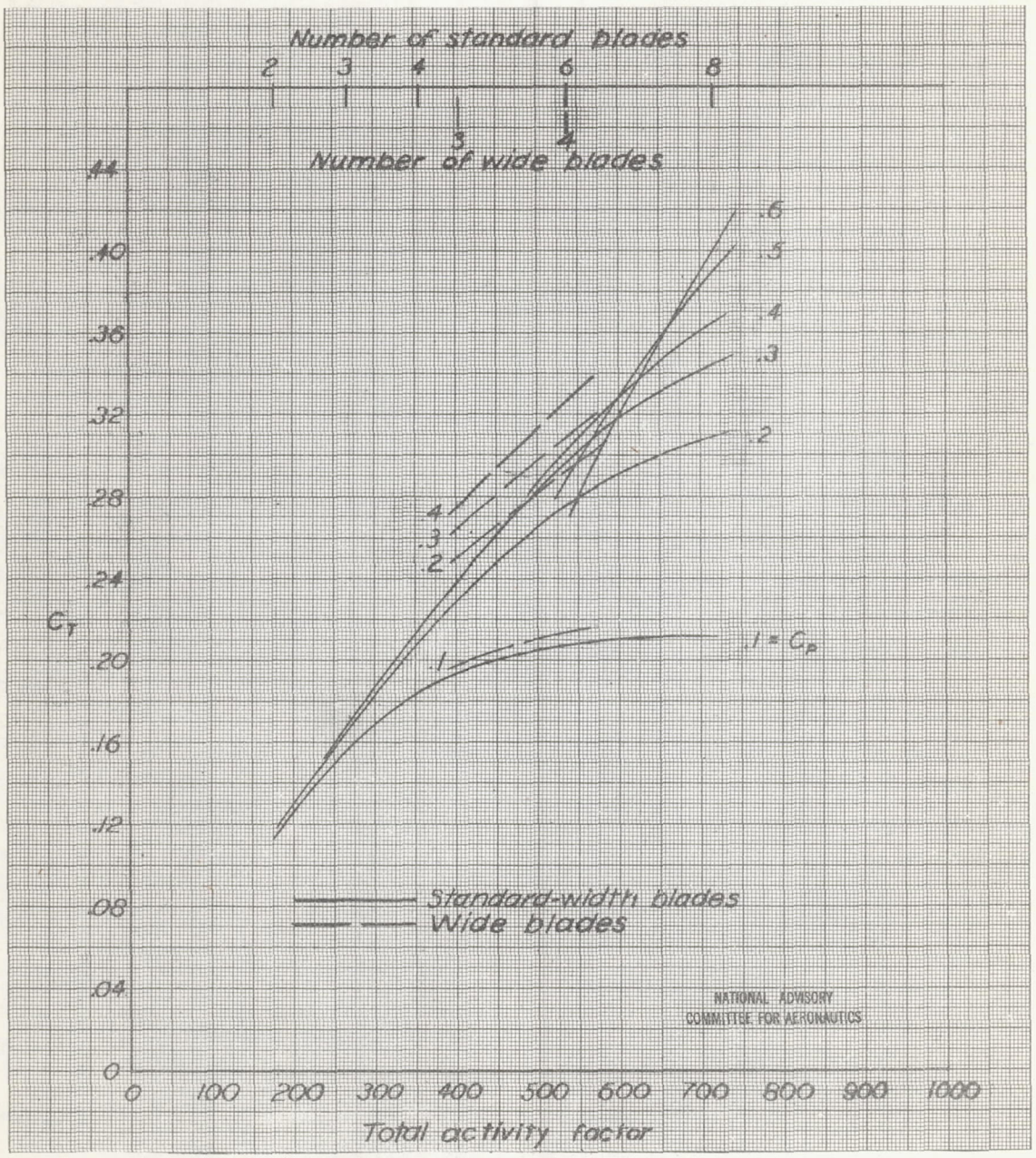
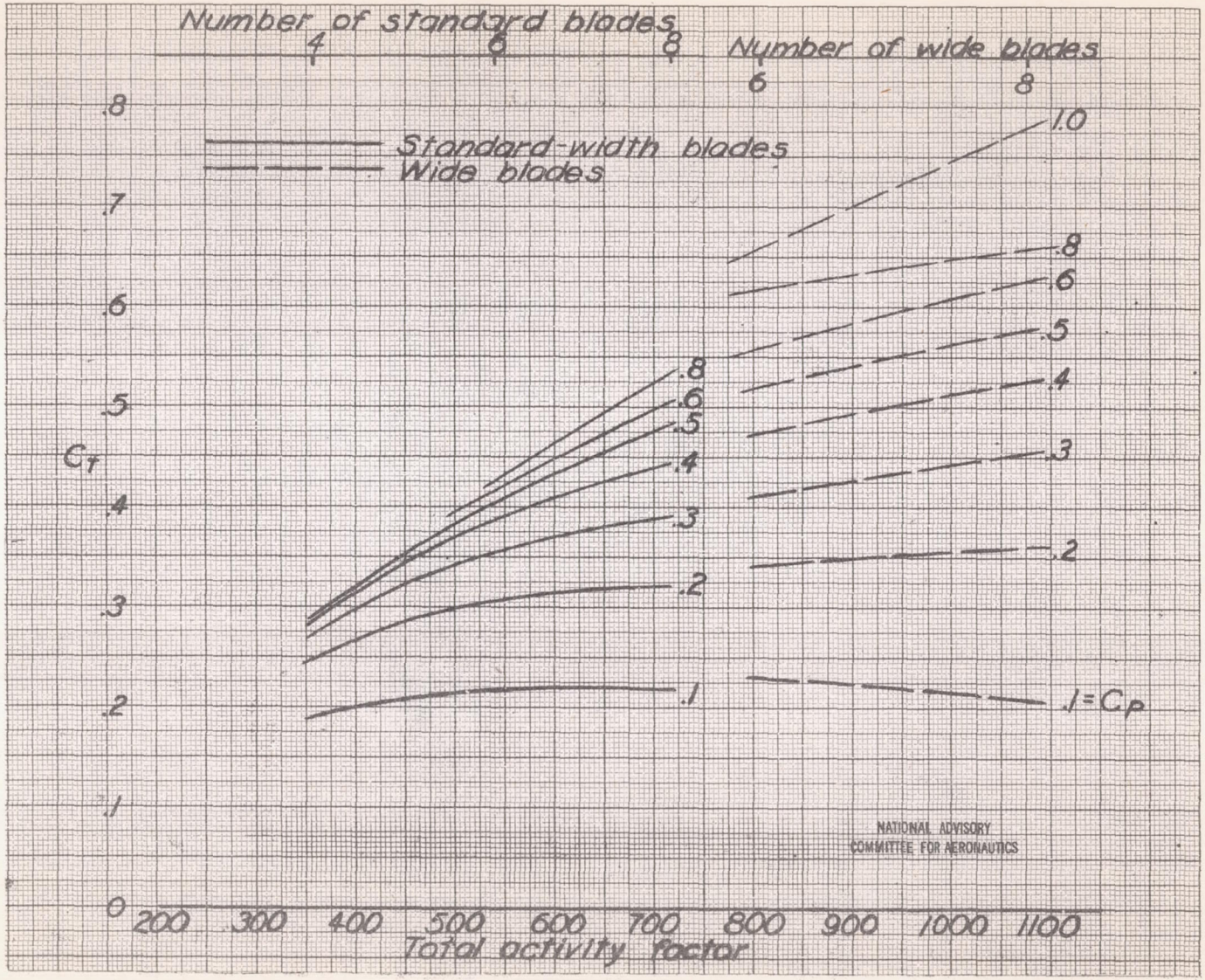


Figure 25.- Comparison of six-blade dual rotating and eight-blade single-rotating propellers on equal power basis. Standard-width blades.



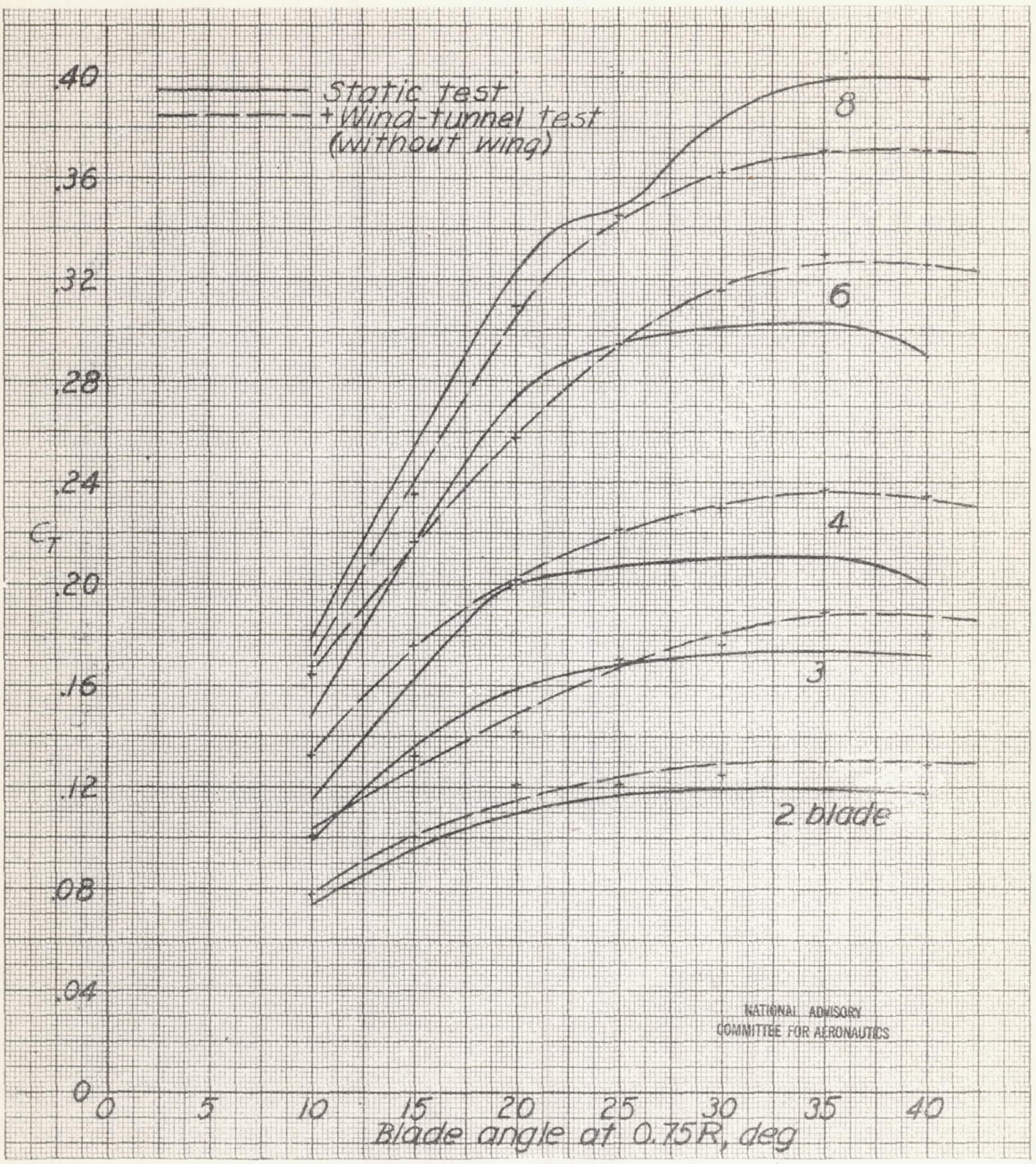
(a) Single-rotating propellers.

Figure 26.- Variation of static-thrust coefficient with activity factor.



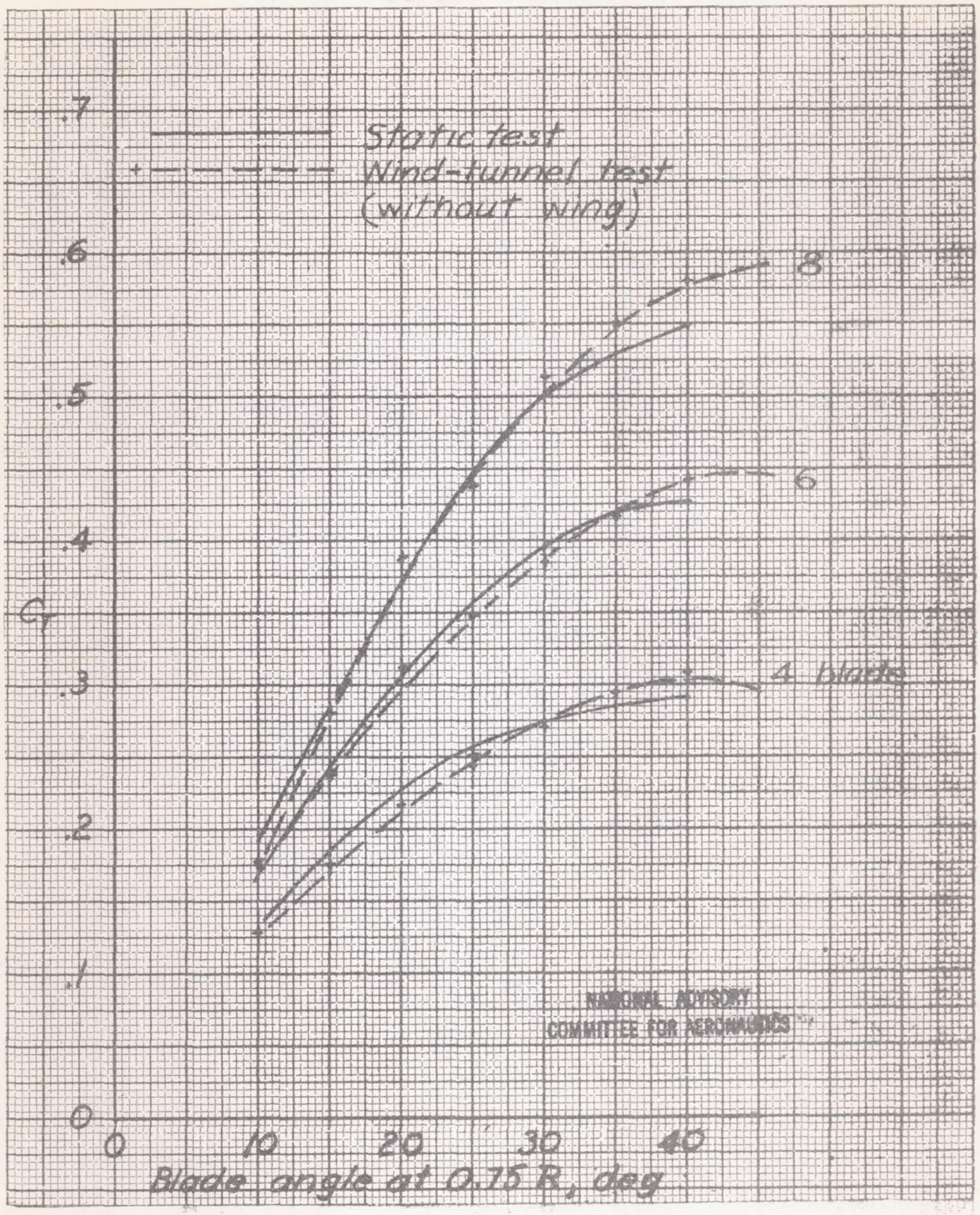
(b) Dual-rotating propellers.

Figure 26.- Concluded.



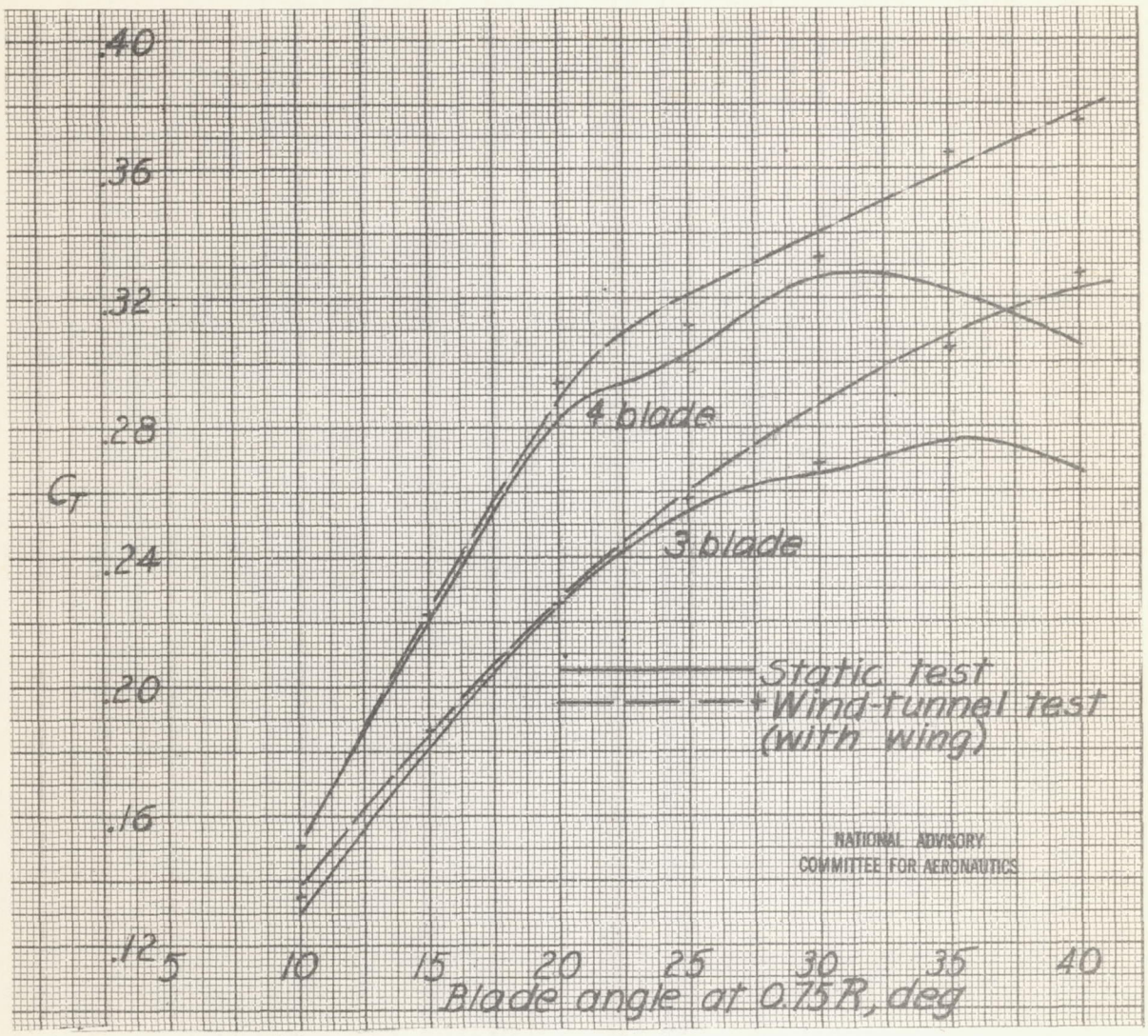
(a) Standard-width blades, single rotation.

Figure 27.- Comparison of static test data and data from extrapolation of wind-tunnel test curves. Thrust coefficient curves.



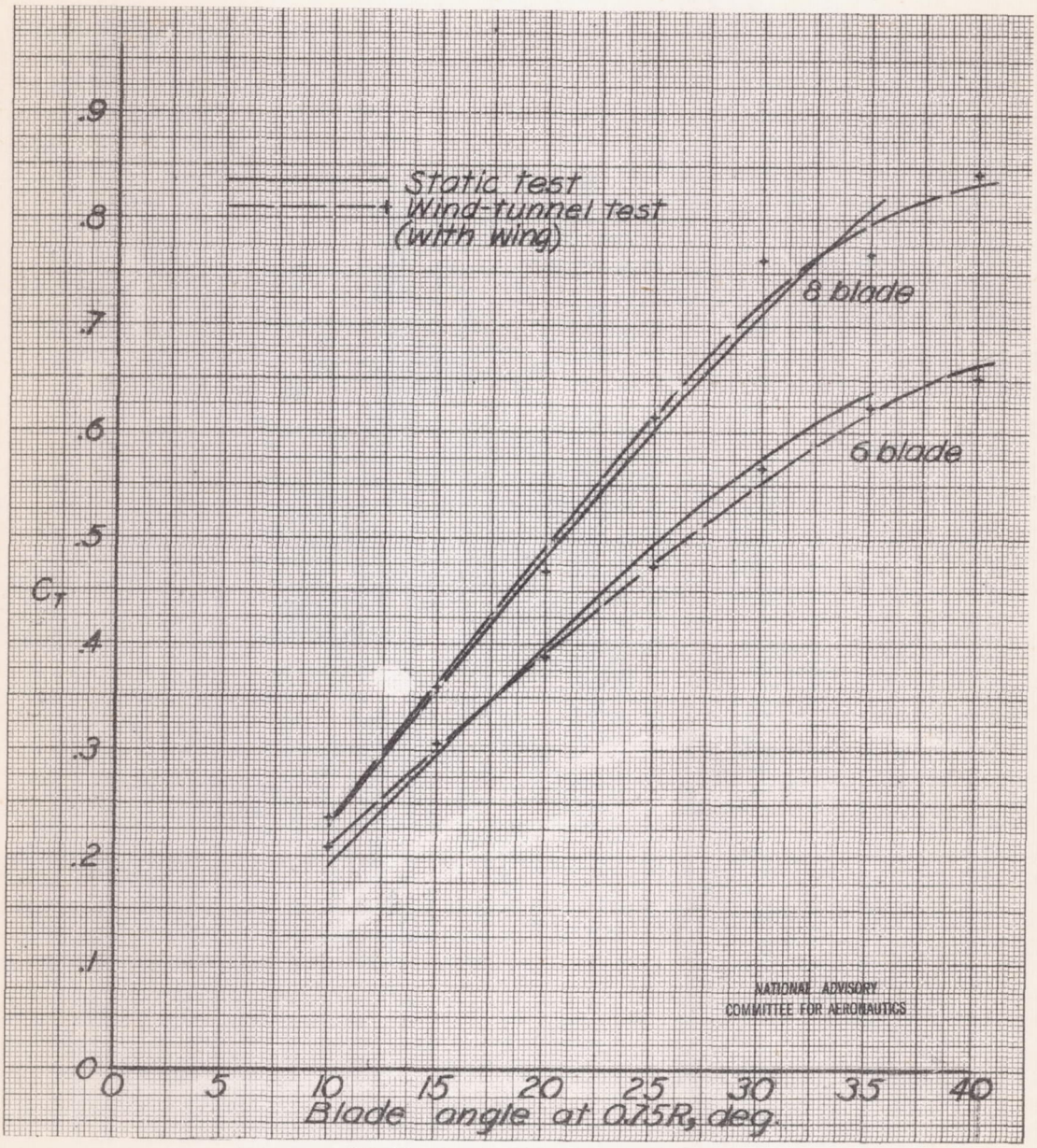
(b) Standard-width blades, dual rotation.

Figure 27.- Continued.



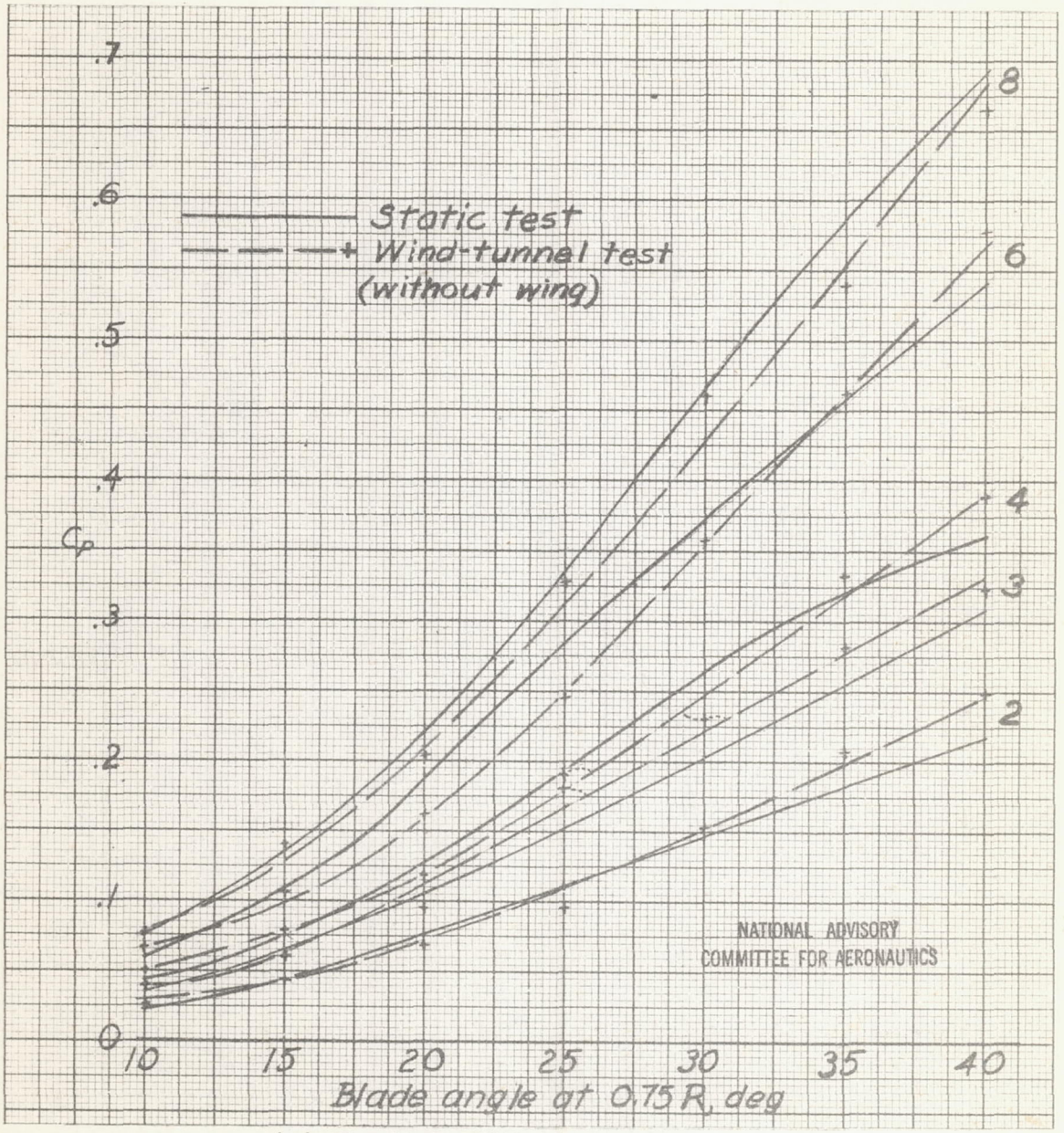
(c) Wide blades, single rotation.

Figure 27.- Continued.



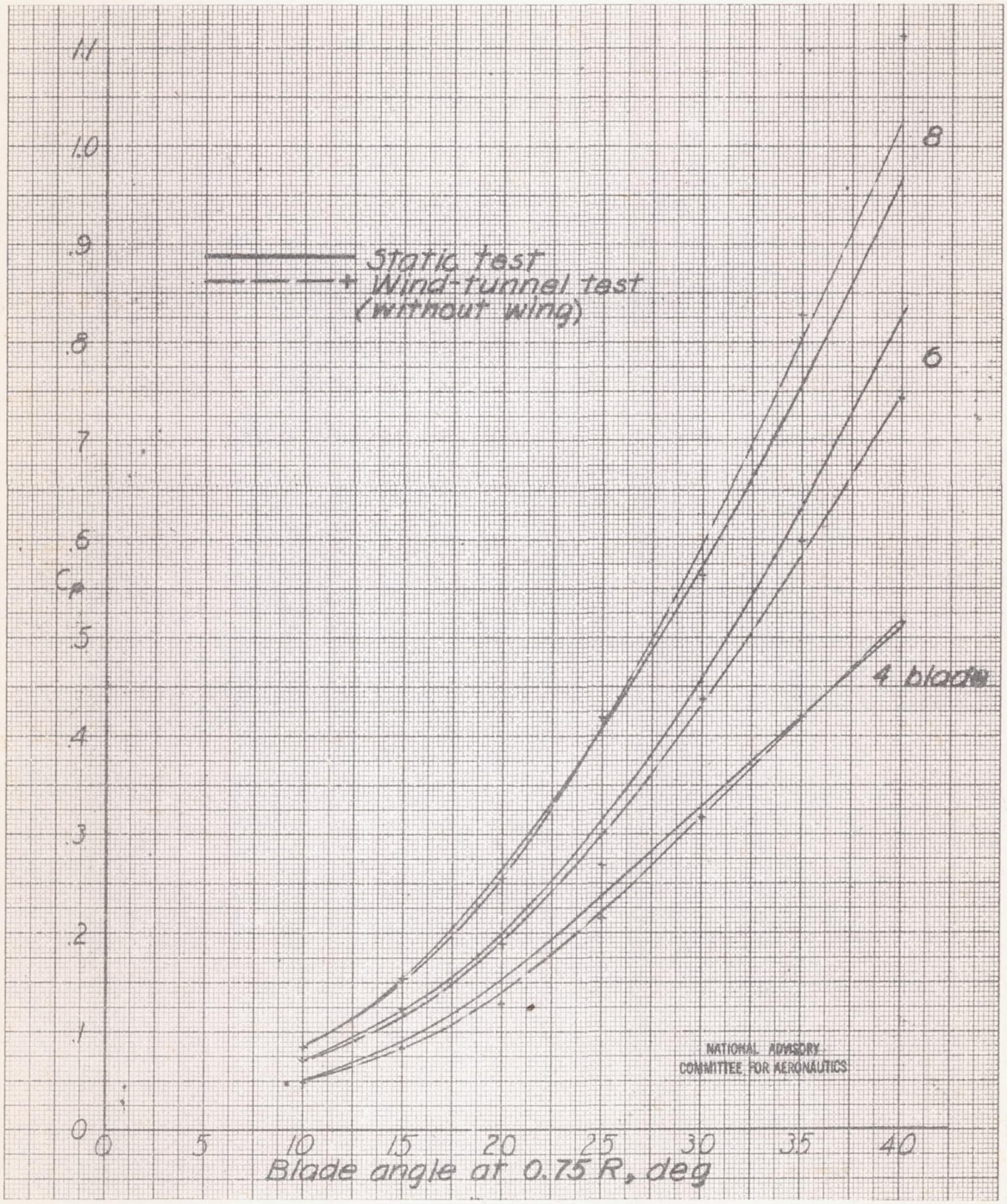
(d) Wide blades, dual rotation.

Figure 27.- Concluded.



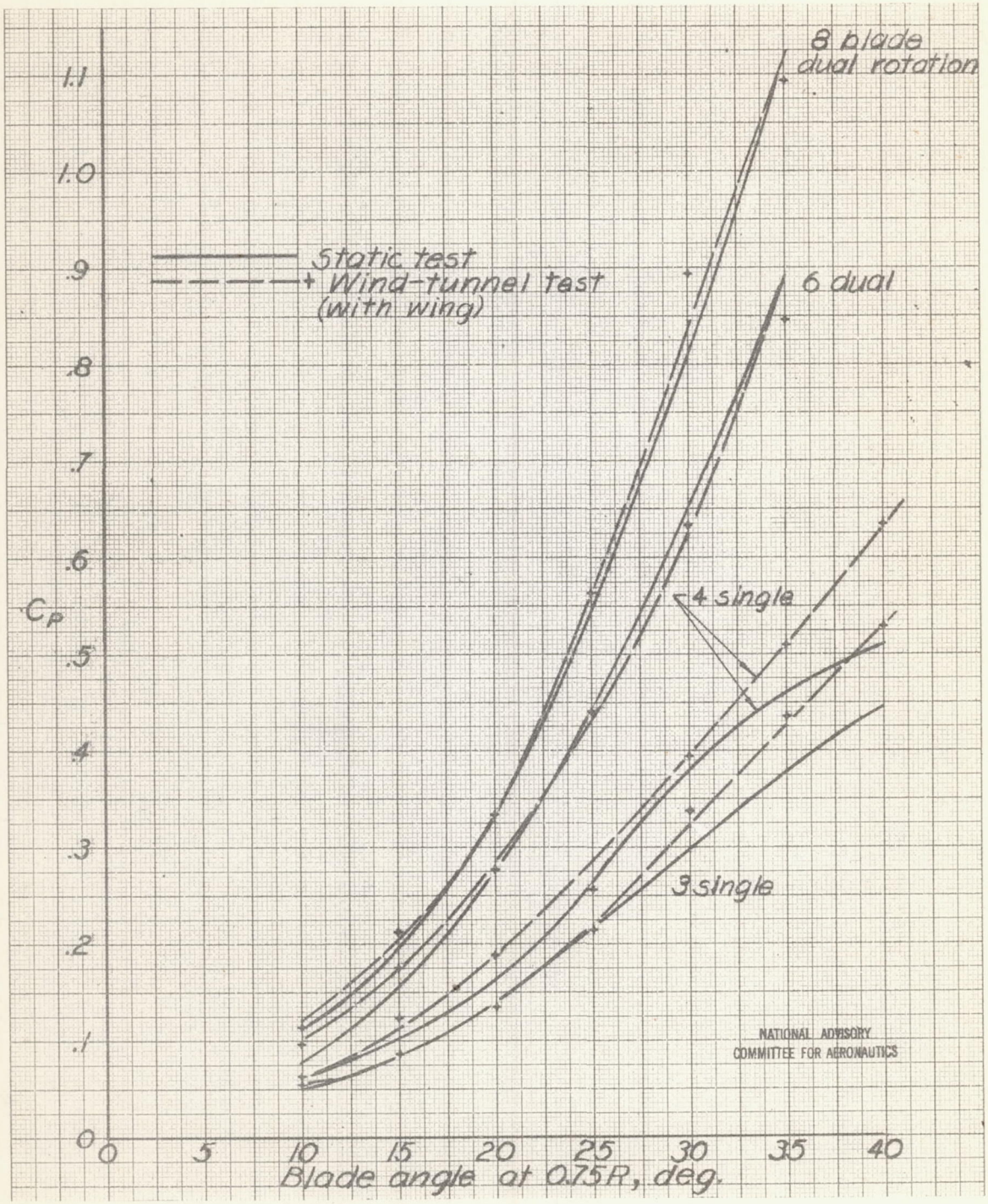
(a) Standard-width blades, single rotation

Figure 28.- Comparison of static test data and data from extrapolation of wind-tunnel test curves. Power-coefficient curves.



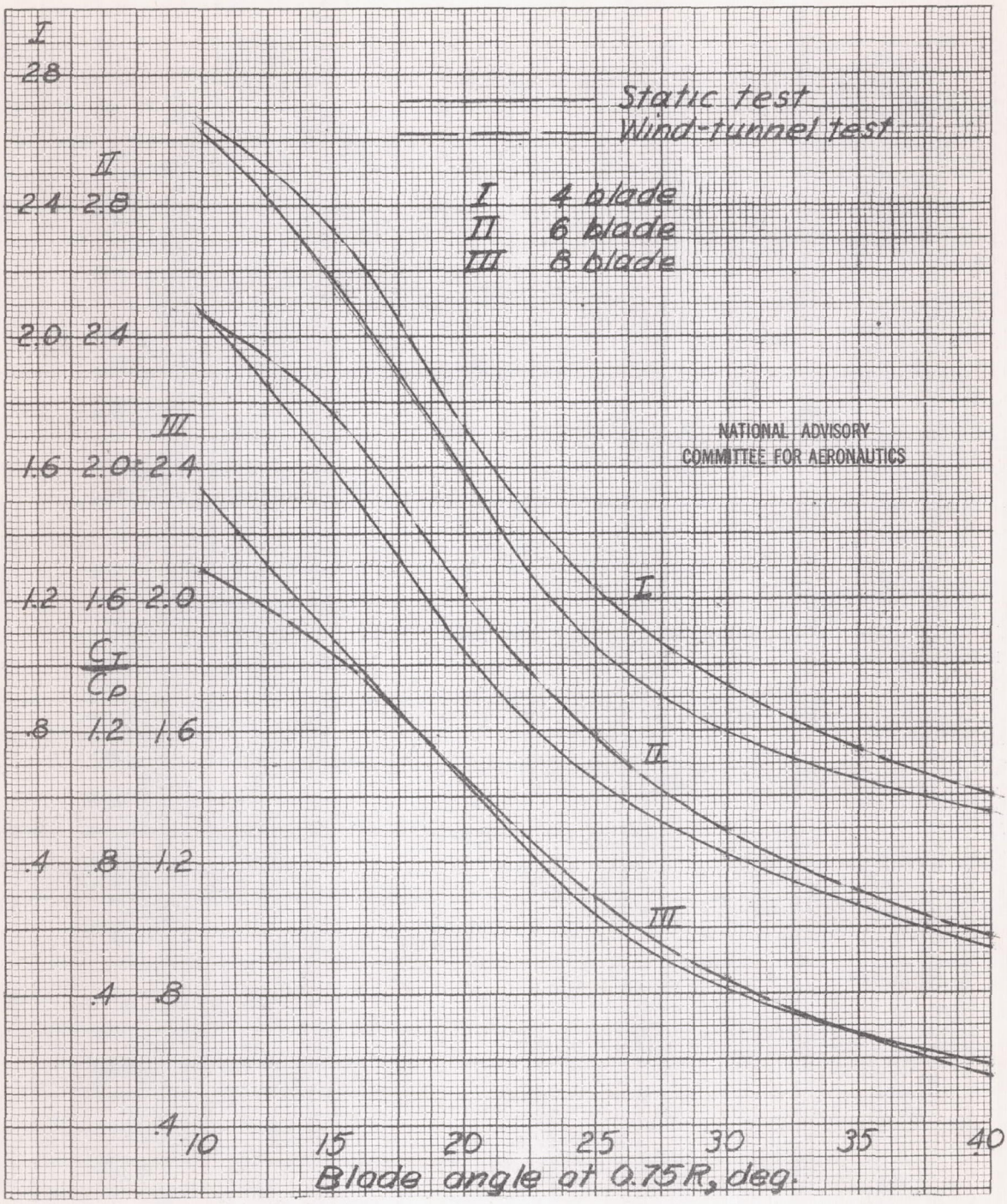
(b) Standard-width blades, dual rotation.

Figure 28.- Continued.



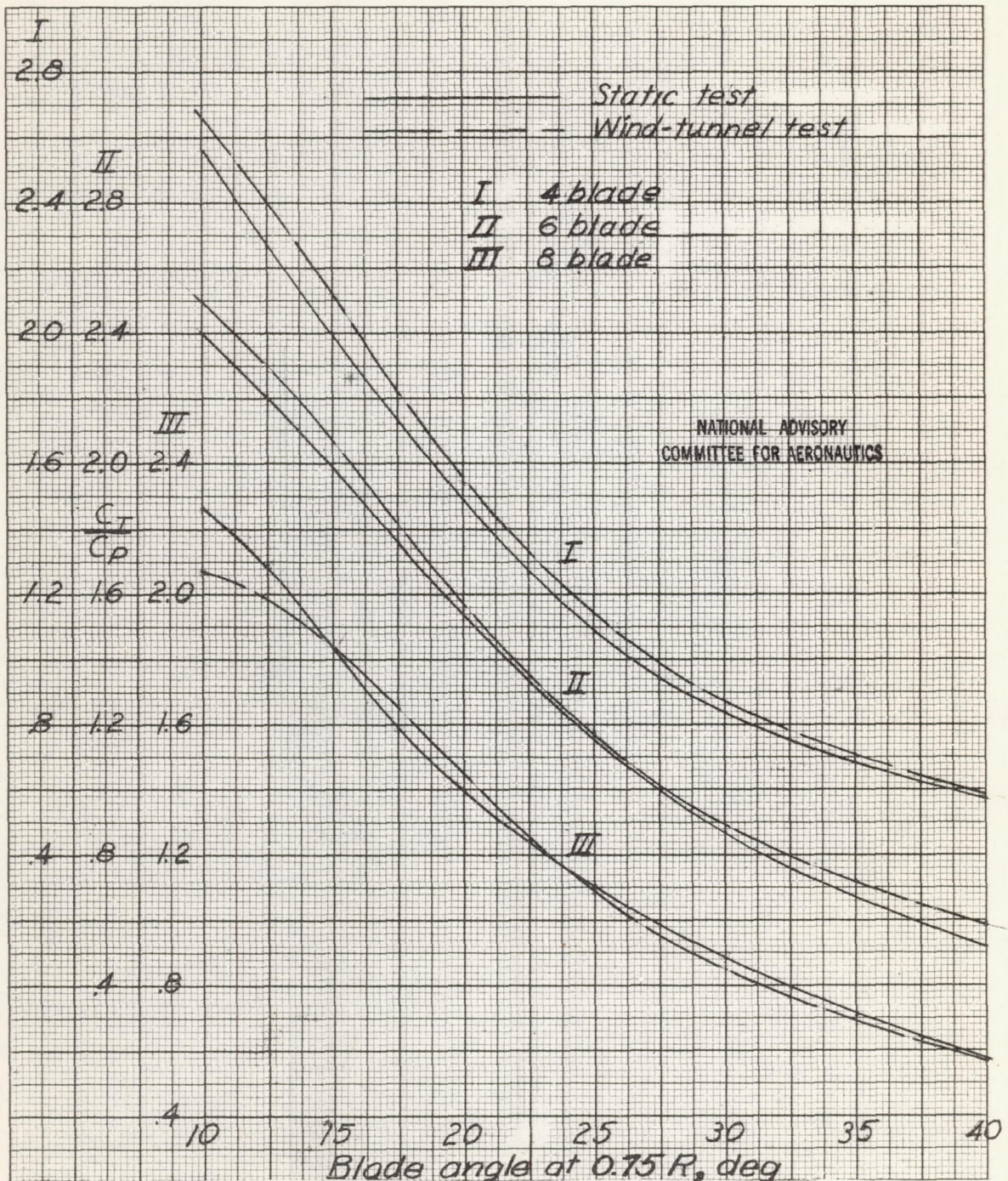
(c) Wide blades.

Figure 28.- Concluded.



(a) Single rotation.

Figure 29,- Comparison of static test data and data from extrapolation of wind-tunnel test curves.



(b) Dual rotation.

Figure 29.- Concluded.

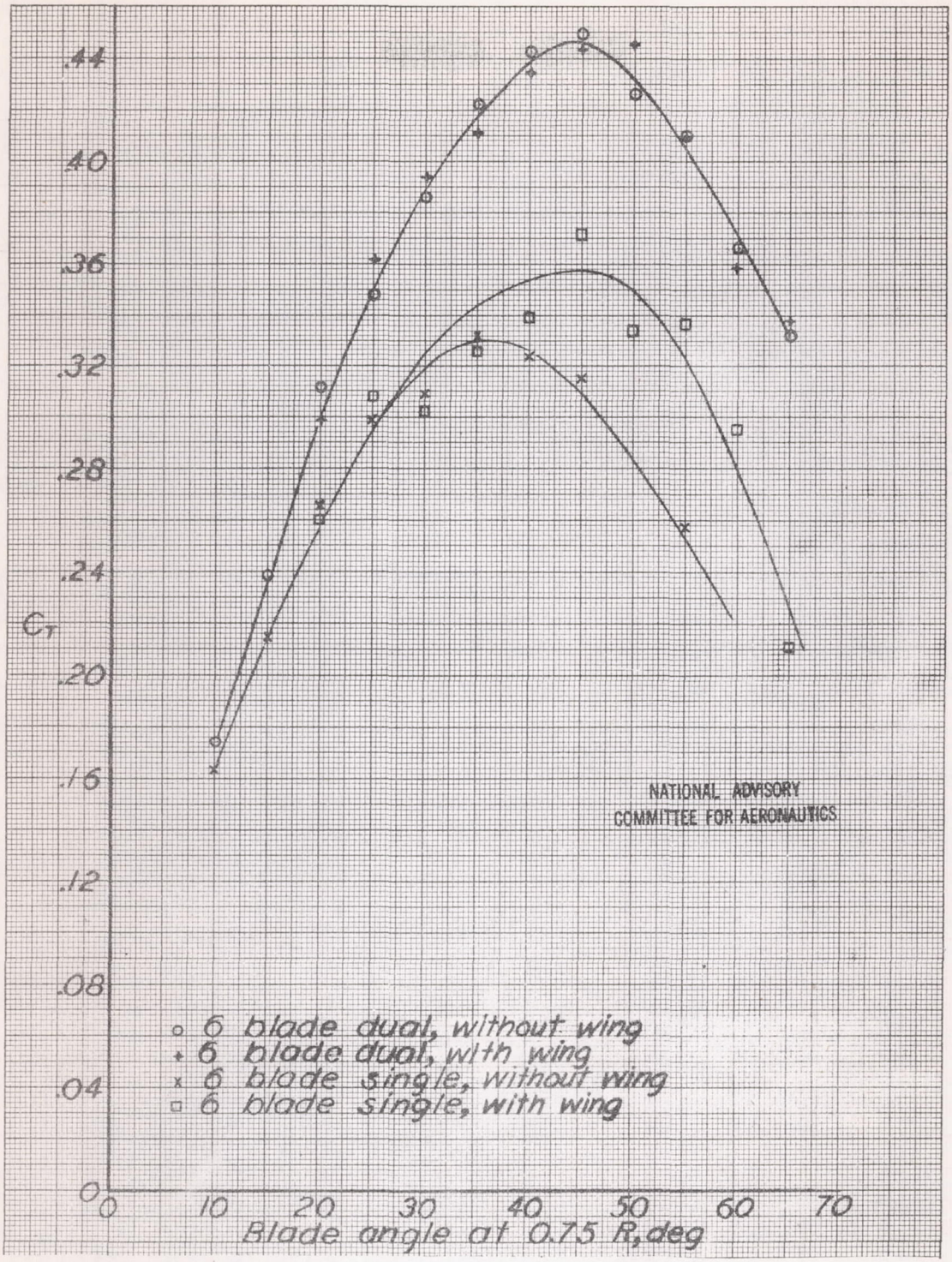


Figure 30.- Static-thrust coefficient curves from extrapolation of wind-tunnel data showing effect of wing on six-blade single- and dual-rotating propellers.

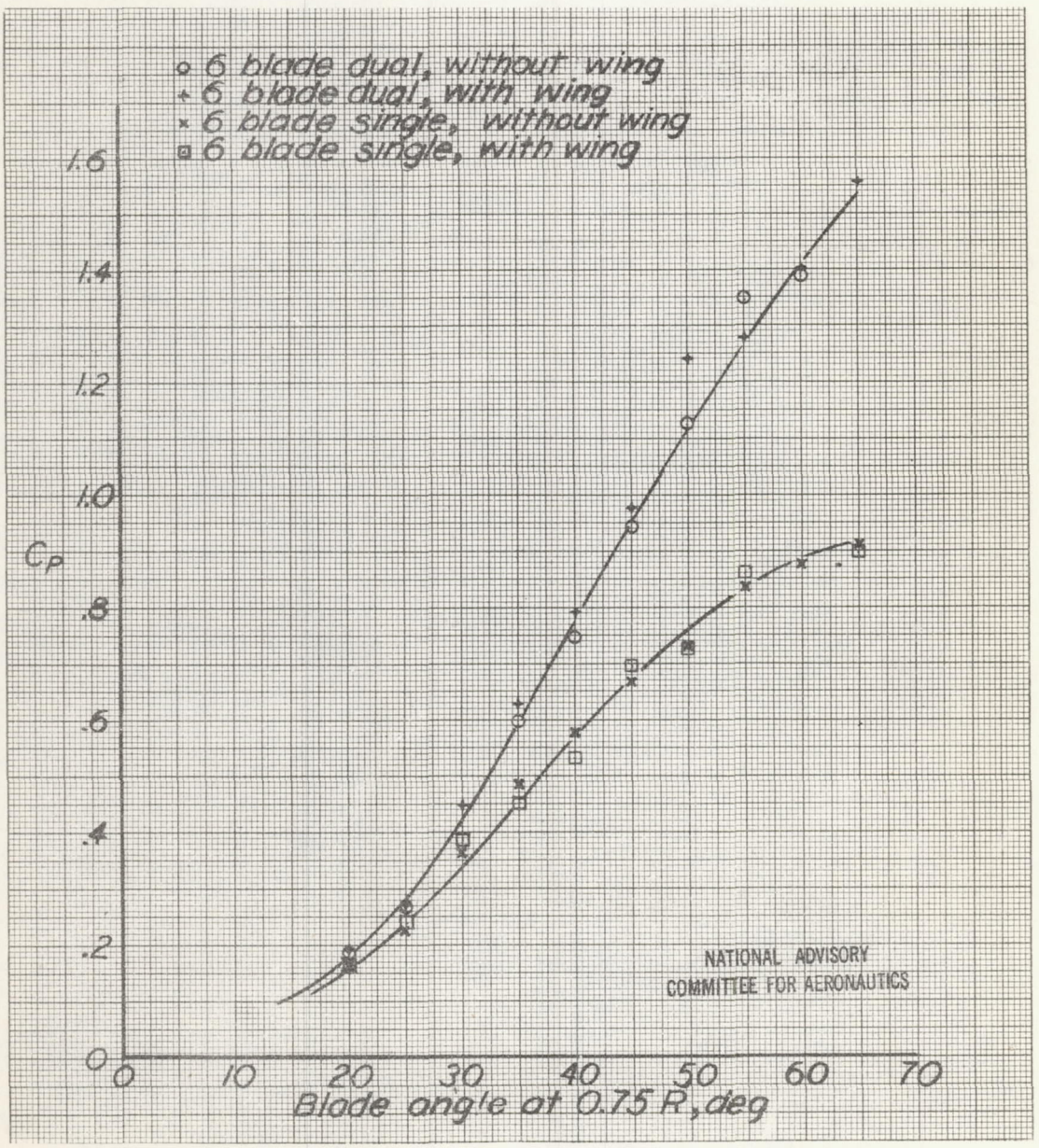


Figure 31.- Static power-coefficient curves from extrapolation of wind-tunnel data showing effect of wing on six-blade single- and dual-rotating propellers.